Molecular Biology of the Cell
Vol. 14, 173–189, January 2003

Osteopontin Deficiency Produces Osteoclast Dysfunction Due to Reduced CD44 Surface Expression

M. A. Chellaiah,*† N. Kizer,‡ R. Biswas,* U. Alvarez,‡ J. Strauss-Schoenberger,‡ L. Rifas,§ S. R. Rittling,¶ D. T. Denhardt,¶ and K. A. Hruska‡

*Department of Oral/Craniofacial Biological Sciences, University of Maryland, Baltimore, Maryland 21201; Departments of ‡Pediatrics and §Bone and Mineral Divisions, Department of Medicine, Washington University School of Medicine, St. Louis, Missouri 63110; and ¶Department of Cell Biology and Neuroscience, Rutgers University, Nelson Labs, Piscataway, New Jersey 08854-8000

Submitted June 20, 2002; Revised September 13, 2002; Accepted September 20, 2002
Monitoring Editor: Keith R. Yamamoto

Osteopontin (OPN) was expressed in murine wild-type osteoclasts, localized to the basolateral, clear zone, and ruffled border membranes, and deposited in the resorption pits during bone resorption. The lack of OPN secretion into the resorption bay of avian osteoclasts may be a component of their functional resorption deficiency in vitro. Osteoclasts deficient in OPN were hypomotile and exhibited decreased capacity for bone resorption in *vitro*. OPN stimulated CD44 expression on the osteoclast surface, and CD44 was shown to be required for osteoclast motility and bone resorption. Exogenous addition of OPN to OPN−/− osteoclasts increased the surface expression of CD44, and it rescued osteoclast motility due to activation of the $\alpha_v\beta_3$ integrin. Exogenous OPN only partially restored bone resorption because addition of OPN failed to produce OPN secretion into resorption bays as seen in wild-type osteoclasts. As expected with these in vitro findings of osteoclast dysfunction, a bone phenotype, heretofore unappreciated, was characterized in OPN-deficient mice. Delayed bone resorption in metaphyseal trabeculae and diminished eroded perimeters despite an increase in osteoclast number were observed in histomorphometric measurements of tibiae isolated from OPN-deficient mice. The histomorphometric findings correlated with an increase in bone rigidity and moment of inertia revealed by load-to-failure testing of femurs. These findings demonstrate the role of OPN in osteoclast function and the requirement for OPN as an osteoclast autocrine factor during bone remodeling.

INTRODUCTION

Osteopontin (OPN) is a phosphorylated glycoprotein synthesized by multiple cell types throughout the body in response to injury and by some cell types as a result of transformation (Sodek *et al.*, 2000; Denhardt *et al.*, 2002; Weber, 2002). In addition, bone cells secrete OPN physiologically during the process of skeletal modeling and remodeling, and it is a major noncollagenous component of bone matrix (Weinreb *et al.*, 1990; McKee *et al.*, 1993; Takano-Yamamoto *et al.*, 1994). The sites of OPN deposition in bone include the lamina limitans at cell-mineralized tissue surfaces, mineralization loci in osteoid, and the organic material at mineralization fronts (McKee *et al.*, 1993; Dodds *et al.*, 1995). Immunolocalization studies have demonstrated OPN in situ in osteoblasts and have shown its accumulation in mineralized bone matrix during endochondral and intramembranous ossification (Reinholt *et al.*, 1990, Hultenby *et al.*, 1991, McKee *et al.*, 1993). Thus, the synthesis, secretion and deposition of OPN in bone remodeling have generally been considered an osteoblast function.

In recent years, multiple investigators have demonstrated that osteoclasts express the message for OPN (Mark *et al.*, 1987; Reinholt *et al.*, 1990; Ikeda *et al.*, 1992; Tezuka *et al.*, 1992; Merry *et al.*, 1993; Takano-Yamamoto *et al.*, 1994; Dodds *et al.*, 1995) and synthesize the protein (Reinholt *et al.*,

Article published online ahead of print. Mol. Biol. Cell 10.1091/mbc.E02–06–0354. Article and publication date are at www.molbiolcell.org/cgi/doi/10.1091/mbc.E02–06–0354.

† Corresponding author. E-mail address: mac001@dental.umaryland.edu.

Abbreviations used: $\alpha_v\beta_3$, vitronectin receptors; OPN, osteopontin; OPN−/−, osteopontin-deficient mice; pQCT, peripheral quantitative computed tomography; CD44s, standard CD44; CD44 v3–10, variant CD44; RANKL, receptor activator of nuclear factor-kappa B ligand; ROK-α, Rho associated kinase- alpha; ERM, erzin-radixin-moesin; mCSF-1, macrophage colony-stimulating factor.

1990; Dodds *et al.*, 1995). Dodds *et al.* (1995) have suggested that osteoclasts may be the source of OPN in the cement lines of bone during remodeling. This is in contrast to the synthesis of OPN by osteoblasts during bone formation. The debate (McKee and Nanci, 1996) focuses the question of osteoclast OPN function during bone resorption, which remains unknown despite recent progress.

We have found that avian osteoclasts secrete OPN from their basolateral cell membranes in vitro, but do not secrete OPN at the ruffled border or into the resorption cavities (Chellaiah and Hruska, 2002). Addition of OPN to osteoclast cultures mimicking secretion from the basolateral surface, stimulated cell shape changes and cytoskeletal rearrangement observed when cell motility is induced. Although polarized secretion of OPN from the basolateral surface of the avian osteoclasts aided in its characterization as an autocrine motility factor, several investigators have shown that OPN is secreted differently in human osteoclasts, osteoclast-like cells derived from human giant cell tumors of bone (GCT), or rodent osteoclasts (Chenu *et al.*, 1994; Maeda *et al.*, 1994; Dodds *et al.*, 1995). Dodds *et al.* (1995) have localized OPN to the resorption pits of osteoclasts in bone and have demonstrated that human GCTs secrete OPN onto the resorption surfaces of dentine. These results are in agreement with the studies carried out in rodent osteoclasts (Maeda *et al.*, 1994). We were able to document this pathway of OPN secretion into resorption bays of osteoclasts isolated from mice. This was in contrast to our findings in avian osteoclasts and demonstrated a species difference in the secretory pathway of OPN. The lack of OPN secretion into the resorption bay may be a mechanism for the functional resorption deficiency of avian cells in vitro (Chellaiah and Hruska, 2002).

OPN contains the arginine-glycine-aspartate (RGD) integrin binding motif, and it functions in cell adhesion related to the osteoclast integrin $\alpha_v\beta_3$ (Reinholt *et al.*, 1990; Flores *et al.*, 1992; Ross *et al.*, 1993). OPN is a potent chemotactic factor acting both as a chemoattractant and as a survival factor during cell motility (Liaw *et al.*, 1994; Soga *et al.*, 2001). We have demonstrated that OPN binding to $\alpha_v\beta_3$ activates a gelsolin-based signal generation complex in osteoclast podosomes that involves Rho activation in the assembly and disassembly of the osteoclast cytoskeleton during motility (Chellaiah *et al.*, 2000a). Thus, the functions of OPN in osteoclasts may be the promotion of cell adhesion and chemotaxis during bone resorption (Reinholt *et al.*, 1990; Weber *et al.*, 1996; Suzuki *et al.*, 2002). However, the absence of a detected bone phenotype in the original report of OPN deficiency raises the question as to the importance of osteoclast OPN as an autocrine factor. We have recently discovered a bone phenotype that was originally missed in gelsolin-deficient mice consisting of a mild osteopetrosis (Chellaiah *et al.*, 2000b). One of the aspects of gelsolin deficiency was the disablement of osteopontin signaling. This caused us to reconsider the importance of OPN as an osteoclast autocrine factor.

Here, we report that osteoclasts deficient in OPN are disabled in motility and bone resorption in vitro. Furthermore, we discovered that exogenous OPN rescues cell motility of OPN null osteoclasts, but only incompletely restores normal bone resorption because exogenous OPN did not appear in the resorption pit. Also, the surface expression of CD44 is reduced in OPN$-/-$ osteoclasts and exogenous OPN or constitutively active Rho partially restored surface expression of CD44. An antibody to β_3 blocked the effect of OPN. Furthermore, a clear defect in bone resorption was detected in a complex skeletal phenotype in OPN-deficient mice. These data demonstrate that OPN is a required osteoclast autocrine mediating CD44 surface expression and regulating osteoclast motility and bone resorption.

MATERIALS AND METHODS

Materials

Antibodies to the standard (monoclonal and polyclonal) and goat (polyclonal) anti-human CD44 variant (v3–10; AHS4441) were purchased from BioSource International Inc. (Camarillo, CA). Rabbit anti-α_v (AB1930) or β_3 (AB1932) antibodies were purchased from Chemicon International Inc. (Temecula, CA). Protein assay reagent kit, reagents for PAGE, and molecular weight standards were purchased from Bio-Rad (Hercules, CA). CY2- or CY3-conjugated anti-mouse, -rabbit, or -goat antibodies were purchased from Jackson ImmunoResearch Laboratories, Inc. (West Grove, PA). Biotin (EZ-link Sulfo-NHS-LC Biotin) and Immunopure HRP-conjugated streptavidin were purchased from Pierce (Rockford, IL). Protein A sepharose, HRP-conjugated mouse, goat, or rabbit IgG, and other chemicals were purchased from Sigma Chemical Co. (St. Louis, MO). mCSF1 was purchased from R&D Systems. Inc. (Minneapolis, MN). pGEX vector containing the cDNA sequences encoding the RANKL was kindly provided by Dr. Steven L. Teitelbaum (Department of Pathology, Washington University School of Medicine, St. Louis, MO). RANKL was purified using the glutathione sepharose (Amersham Biosciences, Piscataway, NJ) as directed by the manufacturers' instructions.

Osteopontin-deficient Mice

The OPN-deficient mouse colony, originally established at Rutgers by homologous recombination in ES cells (Rittling *et al.*, 1998), was rederived at Washington University by caesarian section. The analyses described were performed using wild-type (WT) and osteopontin null (OPN$-/-$) mice on a 129 $\times$ C57BL/6 hybrid background.

Coculture and Generation of Murine Osteoclasts In Vitro

Mouse osteoclasts were generated in vitro using mouse bone marrow cells as described previously (Chellaiah *et al.*, 2001). After 3 d in culture osteoclasts were generated in cultures supplemented with mCSF1 (10 ng/ml) and RANKL (55–70 ng/ml). Multinucleated osteoclasts were observed from day 4 onward. About 90–95% TRAP- positive osteoclasts were observed from day 5 onward. To remove the osteoclasts for in vitro bone resorption or motility studies, cells were washed with PBS and kept in a cell stripper solution (Cellgro by Media Tech, Inc., Herndon, VA) for 15–30 min. Cell stripper is a nonenzymatic cell dissociation solution designed to gently dislodge adherent cells in tissue culture. After incubation with the cell stripper solution, osteoclasts were removed from the plates by gentle scraping. Some of the removed cells were replated and stained with either trypan blue or for tartrate-resistant acid phosphatase (TRAP). Cells excluded trypan blue, and they were 99% TRAP positive. These TRAP-positive cells were used for migration and bone resorption assays as described below.

Purification of Osteopontin Protein

Mouse OPN cDNA was cloned into *Bam*HI/*Xba*I site of pQE 30 vector (Qiagen Inc., Valencia, CA). OPN was expressed as a 6-His–tagged protein. OPN was purified from the bacterial lysate using

Ni-NTA affinity chromatography following the manufacturer's instructions (Qiagen Inc.).

Lysate Preparation and Western Analysis

Purification and transduction of Tat-fusion proteins into osteoclasts were performed as described previously (Chellaiah *et al.*, 2000 b). After treatments with Tat fusion proteins or OPN, cells were washed three times with ice-cold phosphate-buffered saline (PBS) and added with RIPA lysis buffer (10 mM Tris-HCl, pH 7.2, 150 mM NaCl, 1% deoxycholate, 1% Triton X-100, 0.1% SDS, 1% aprotinin, and 2 mM PMSF; Chellaiah and Hruska, 1996). Cells were rocked on ice and transferred to Eppendorf tubes. The lysates were centrifuged at 15,000 rpm, and the supernatant was saved. Protein contents were measured using the Bio-Rad protein assay reagent kit. Equal amounts of lysate proteins from WT and OPN−/− osteoclasts were used for immunoprecipitation and Western analysis with anti-CD44 antibody (Chellaiah and Hruska, 1996).

Biotinylation

After 4 or 5 d in culture, the osteoclast precursors made from WT or OPN−/− mice were kept in serum-free media for 2 h. Subsequently, each plate was treated with TAT proteins or OPN as described above. Cells were washed with PBS and labeled with biotin according to the manufacturer's guidelines (Pierce, Rockford, IL). Briefly, osteoclasts were incubated with 0.5 mg/ml biotin for 30–40 min at room temperature. Cells were washed two or three times with cold PBS and lysed with RIPA buffer (Chellaiah and Hruska, 1996). Equal amount of proteins were used for immunoprecipitation with a polyclonal CD44 antibody (Biosource International Inc., Camarillo, CA). The immune complexes were subjected to SDS-PAGE, and the proteins were transferred to a PVDF membrane for immunoblot analyses. Blots were blocked with 10% milk in PBS containing 0.5% Tween (PBS-T) for 2–3 h and then incubated with a 1:500 dilution of peroxidase-conjugated streptavidin for over night at 4°C. After three washes for 10 min each with PBS-T, protein bands were visualized by chemiluminescence using the ECL-kit (Pierce).

Cell Migration Assays

Phagokinesis and chemotaxis (transwell migration) assays were performed as described (Takaishi *et al.*, 1995; Chellaiah *et al.*, 2000b). For phagokinesis assay, substrates such as recombinant mouse OPN, vitronectin (VN), or fibronectin (FN) were diluted in PBS and used for phagokinesis assays, which were performed in six-well tissue culture dishes. Colloidal gold particles were made essentially as described (Takaishi *et al.*, 1995). Osteoclasts were seeded at low density, and the test substance was added as a soluble protein (OPN, 25 μg/ml; VN, 10 μg/ml; GRGDS, 50 μg/ml) to the α-MEM medium containing 1% serum and 2% BSA. Some wells were treated with an antibody to OPN, β_3, or CD44 (25 μg/ml) in addition to OPN protein. Osteoclasts phagocytized the colloidal gold particle during migration and generate white tracks free of the gold particle. Areas were measured after 14-h incubation with the indicated proteins at 37°C. The migrating cells were visible as a black body. Cell motility was evaluated by measuring the areas free of gold particles. By using a grided reticle (Boyce Scientific, Inc., Gray Summit, NC) in the eyepiece of a Nikon microscope, areas free of gold particles were measured using a 10× objective and represented as area moved in mm^2.

To assay chemotaxis migration, transwell chambers with membranes of 8-μm pore size (Costar, Cambridge, MA) were used (Senger *et al.*, 1996). The undersides of the membranes were coated with vitrogen 100 (collagen type 1; 30 mg/ml) at room temperature for 2 h, as directed by the manufacturer's instructions. Cells were added to the upper chamber in α-MEM medium containing 1% serum and 2% BSA (100 μl) and the test substrate (OPN, 25 μg/ml; VN, 10 μg/ml; GRGDS, 50 μg/ml) was added to the lower chamber in the same medium (600 μl). Antibody to OPN, CD44, or β_3 (25 μg/ml) was added to the upper chamber. Cell migration was allowed to proceed at 37°C in a standard tissue culture incubator for 12–14 h. Cells that migrated to the undersides were stained for tartrate-resistant acid phosphatase and visualized and counted in a Nikon microscope using a 10× objective. Data are presented as the number of migrated cells/field (mean ± SE), and all assays were performed in quadruplicates. Statistical significance was calculated as mentioned below in data analysis.

Bone Resorption Assay

Bone resorption assay was performed as described previously (Chellaiah *et al.*, 2000b). The osteoclast suspension (2×10^4 cells) was added to each well and after 2 h of adherence, the culture medium was replaced with α-MEM medium containing either TAT-fusion proteins as indicated in Figure 8 to a final concentration of 100 nM or OPN (10 μg/ml). Some wells were added with an antibody to OPN, CD44, or integrin α_v or β_3 (10–25 μg/ml) and OPN protein (25 μg/ml). Medium was replaced with the respective protein or antibody after 24 h. After 48 h, cells were scrapped from dentine and the slices were washed two times with water. Dentine slices were stained with acid hematoxylin (Sigma) and washed with water. Pits were viewed under 40× objective in a phase contrast microscope and photographed.

Immunostaining

Osteoclasts cultured on whale dentine slices or glass coverslips were immunostained with the indicated antibodies in the results section as described (Chellaiah *et al.*, 1996, 2000b). To visualize the surface expression of CD44, osteoclasts were fixed with paraformaldehyde, rinsed with cold PBS, and incubated with a mAb to CD44 antibody (1:100 dilution) for 2–3 h without permeablization with Triton X-100. Cells were washed and counterstained with Cy2- or Cy3-conjugated secondary antibodies for 2 h. After washing few times with PBS, osteoclasts were mounted on a slide in a mounting solution (Vector Laboratories, Inc., Burlingame, CA). The immunostained cells were viewed and photomicrographed on a Zeiss LSM 410 confocal laser-scanning microscope (Thornwood, NY). CY2 and CY3 images were recorded using the 488 nm and 568 argon excitation lines, respectively. The background (bone) is shown by the reflected light in red (pseudocolor) in Figure 1A (bottom panel). CY2- and CY3-labeled proteins were imaged with dual fluorescence mode. Images were stored in TIF image format and processed by the Adobe Photoshop software program (Adobe Systems, Inc., Mountain View, CA).

pQCT Measurement of the Femoral Bone Density and Area of WT and OPN−/− Mice

Bone density and area were calculated using a peripheral quantitative computed tomography system (pQCT; Norland Medical Systems, White Plains, NY). Two sections (0.5 mm beam width) were scanned immediately distal to the growth plate of the femoral head. Trabecular bone was defined as having a density of between 270 and 630 mg/ml. Cortical bone of the metaphysis was defined as having a density above 630 mg/cm^3. The area and average density of cortical and trabecular bone from the two sections was calculated using these parameters and averaged.

Bone Histomorphometry

The tibia were fixed in phosphate-buffered 10% formalin, pH 7.4, and decalcified in 14% EDTA for 10–14 d. Bones were washed sequentially with 50, 70, and 90% ethanol and embedded. longitudinal sections of 5-μm thickness were made and stained with TRAP

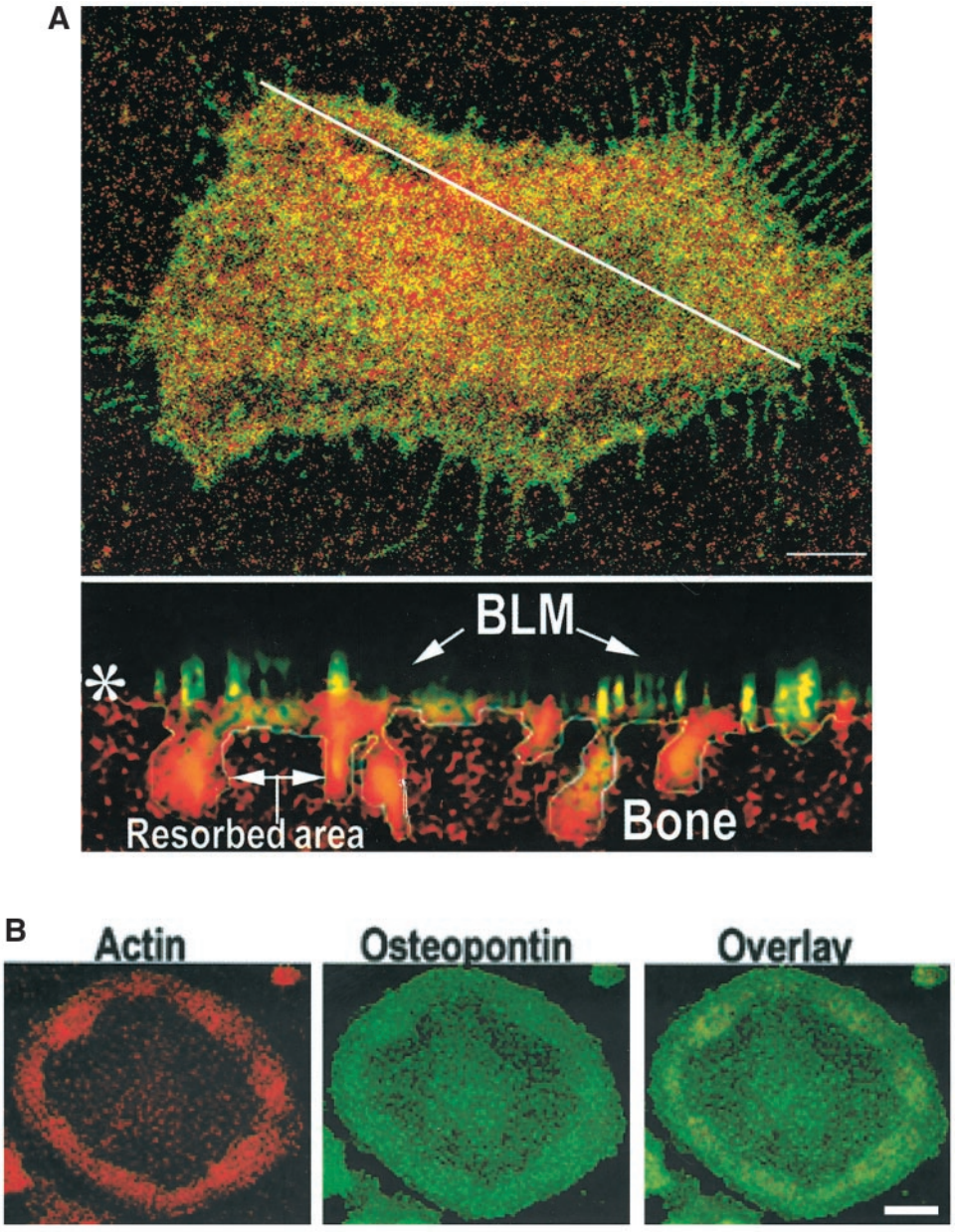

Figure 1. Distribution of OPN and $\alpha_v\beta_3$ integrin in resorbing murine osteoclasts. (A) Top: Osteoclasts plated on bone were immunostained with an antibody to β_3 integrin (green) and OPN (red) and analyzed by confocal laser scanning microscopy. The diagonal white line indicates where the XZ scan (bottom panel) was made. Bar, 25 μm. Bottom: Lateral (XZ) confocal view of the osteoclast shown at the top. Basolateral membrane (BLM), and resorbed area are indicated by arrows. Colocalization (yellow) of OPN and $\alpha_v\beta_3$ was seen at the basolateral and ruffled border membranes. The bone is shown by the reflected light in red (pseudocolor). Asterisk (*) indicates the bone surface. (B) Distribution of OPN and actin in osteoclasts plated on glass coverslips. Osteoclasts plated on glass coverslips were immunostained with anti-OPN (green) and stained with rhodamine phalloidin for actin (red). Cells were viewed by confocal microscopy. Bar, 25 μm.

staining to identify osteoclasts. To estimate mineral apposition rate and bone formation rate, mice were injected with calcein at 2 and 7 d before sacrificing. The right distal femur was kept in 90% ethanol and embedded. Longitudinal sections were made. Static and dynamic histomorphometric measurements were made using a computer and digitizer tablet (Osteomeasure; Osteometrics Inc., Atlanta, GA) interfaced to a Leitz microscope (Leitz, Wetzlar, Germany) with a drawing tablet. All measurements were done to the metaphyseal region distal to the growth plate region. To estimate bone formation rate, double-labeled and single-labeled areas were traced and calculated as described (Jilka *et al.*, 1996; Weinstein *et al.*, 1997). Terminology used is that recommended by the Histomorphometry Nomenclature Committee of the American Society of Bone and Mineral Research (Parfitt *et al.*, 1987).

Mechanical Testing of Femurs from OPN+/+ and OPN−/− Mice

Left femora from WT and OPN−/− mice were designated for biomechanical testing. Femora were isolated, cleaned of soft tissues, wrapped in gauze that was soaked with PBS, wrapped again in plastic, placed in a sealed vial, and stored at −20°C until testing. Before testing, specimens were thawed to 23°C. Four-point bending tests were conducted using materials testing machine (Comten Industries, Penellas Park, FL) fitted with an appropriate load transducer (400 N force cell, Comten Industries) and linear variable differential transformer (LVDT; G. L. Collins, Long Beach, CA) for displacement measurement. Tests were conducted using a four-point fixture with 9-mm spacing between the outer (support) points

and 5-mm spacing between the inner (loading) points. The bones were flexed in the anterior-posterior plane. The inner points were displaced at a constant rate of 0.1 mm/s. Force-displacement data were collected using a computerized data acquisition system (software written by Neil Kizer, analog to digital converter from BSOFT Software (Columbus, OH).

After testing, force values (F) from the bending tests were converted to bending moment values (M) using the relation $M = Fa/2$, where a was the distance between the outer and inner points (2.0 mm). Normalized displacement (Nd) was calculated by dividing displacement at the loads by the geometric factor $\{(3aL - 4a^2)/6\}$ to allow direct comparison between other experiments done using different testing geometry's. L is the distance between outer points a (9.0 mm) resulting in a correction factor for our geometry of 6.333. After normalization $Nd = Fa/EI$, which can be calculated for any 4-point bending geometry. In the preceding equation E is the elastic modulus and I is the cross-sectional moment of inertia. From the moment vs. normalized displacement curves four parameters were computed: ultimate moment (Nmm), bending rigidity (Nmm^2), displacement at failure (mm/mm^2) and energy to failure ($Nmm^*[mm/mm^2]$). Failure was defined at the point of ultimate (maximum) moment, and bending rigidity was defined as the slope of the linear region of the curve. The elastic modulus (Young's modulus) was calculated by dividing the four-point bending rigidity by the cross-sectional moment of inertia (I) at the midpoint of the diaphysis. This calculation is the equivalent of finding the slope of the stress vs. strain curve. The moment of inertia was determined by analysis of pQCT images using the Section Maker software package (Formation Design Systems, Fremantle, WA 6959, Australia).

Data Analysis

All comparisons were made as "% control," which refers to vehicle-treated cells. The other treatment groups in each experiment were normalized to each control value. Data presented are means ± SEM of experiments done at different times normalized to intraexperimental control values. For statistical comparisons, analysis of variance (ANOVA) was used with the Bonferroni corrections (Instat for IBM, version 2.0; Graphpad Software, San Diego, CA)

RESULTS

Cellular Localization of OPN and Integrin $\alpha_v\beta_3$ in Resorbing Osteoclasts

The $\alpha_v\beta_3$ integrin was previously shown to localize in the osteoclast plasma membrane opposite to the bone matrix, in the ruffled border (Lakkakorpi and Vaananen, 1991; Zhao *et al.*, 2001) and in the clear zone of osteoclasts (Flores *et al.*, 1992; Hughes *et al.*, 1993; Nesbitt *et al.*, 1993; Nakamura *et al.*, 1996). Therefore, OPN costaining with integrin β_3 was performed in mouse osteoclasts plated on dentine slices to localize OPN staining at the different membrane domains of resorbing osteoclasts. OPN (red) staining was detected at the basolateral surface (Figure 1A, top panel) and ruffled border regions (Figure 1A, bottom panel) of osteoclasts. Basolateral surface OPN staining (red) was punctate and colocalized (yellow) with β_3 (green) in some areas. The diagonal white line in the top panel of Figure 1 indicates location of the XZ scanning. In the lateral view of the osteoclast in the XZ scan (bottom panel), punctate areas of colocalization of β_3 and OPN were observed at the basolateral surface and diffuse OPN staining was observed in the area of resorption (perhaps in the ruffled border). The white line outlines the resorbed area. The bone is shown by the reflected light in red (pseudocolor).

The localization of OPN was also analyzed in osteoclasts plated on glass coverslips. To demonstrate the localization of OPN in the clear zone area of osteoclasts, OPN distribution was compared with the localization of actin. Punctate OPN (green) staining was seen throughout the cell, and both actin and OPN staining were observed at the periphery in the clear zone area where podosomes are located. The significance of colocalization (overlay) of OPN (green) with actin (red) at the periphery in the clear zone area (Figure 1B) of osteoclasts is not known.

Because immunostaining for OPN was observed at the ruffled border of mouse osteoclasts, it was critical to determine whether the OPN expressed at the ruffled border surface was deposited in the resorption pit. After osteoclasts were removed, dentine slices were immunostained using an antibody to OPN. In Figure 2A, serial 2-μm sections of resorption pits generated by osteoclasts derived from WT mice were taken beginning at the dentine surface (0 μm) and progressing through to the bottom of the deepest pit (52 μm). OPN is not present in dentine, and the immunostaining of dentine alone was negative. Dentine slices cultured with osteoclasts demonstrated positive staining for OPN in the resorption pits, indicating OPN to be of osteoclast origin. OPN deposition was seen up to the 48-μm section of the deep pit (Figure 2A). The pit was broader at the surface and narrowed at the bottom. OPN staining followed the contour of the pit. Staining intensity was greater at the top and less intense at the 48-μm depth (indicated by arrow). Enlarged views of resorption pits at 4 and 16 μm are shown in Figure 2B. OPN staining was observed both at the rim at 4-μm section (indicated by arrows) as well as at the shoulder-like structure in the deep resorption pit section at 16-μm depth and the bottom of the other pits (arrows).

In Vitro Bone Resorption Assays

Because addition of soluble OPN stimulated changes in cell shape, cytoskeletal rearrangement, motility, and bone resorption in osteoclasts isolated from chicken and WT mice (Chellaiah *et al.*, 2000a, 2000b), osteoclasts isolated from OPN-null mice were subjected to bone resorption and motility assays in the presence and absence of OPN. OPN was added as soluble protein to the culture medium.

Osteoclasts derived from WT and OPN−/− mice were plated on dentine slices and treated with PBS (vehicle) or OPN. The resorption pits generated by osteoclasts derived from OPN−/− mice were very small (Figure 3, C and G) compared with osteoclasts from WT mice (Figure 3, A and E). OPN treatment restored the formation of multiple overlapping pits (Figure 3, D and H), which is produced by the simultaneous process of motility and resorption, to the levels observed in pits produced by WT osteoclasts (Figures 3, B and F). The depth (XZ scan) and area (XY scan) of the pits were assessed by confocal microscopy (Table 1). The pits produced by OPN−/− osteoclasts were superficial despite the addition of OPN (Figures 3H; Table 1), whereas OPN treatment stimulated pit area and pit depth in osteoclasts derived from WT mice (Figure 3F; Table 1) in agreement with our previous reports (Chellaiah *et al.*, 2000b). Although the increase in pit depth was significant in OPN-treated WT osteoclasts compared with OPN−/− osteoclasts, there were no significant differences in the pit area. The observations made in Figure 3 were consistent across multiple osteoclast

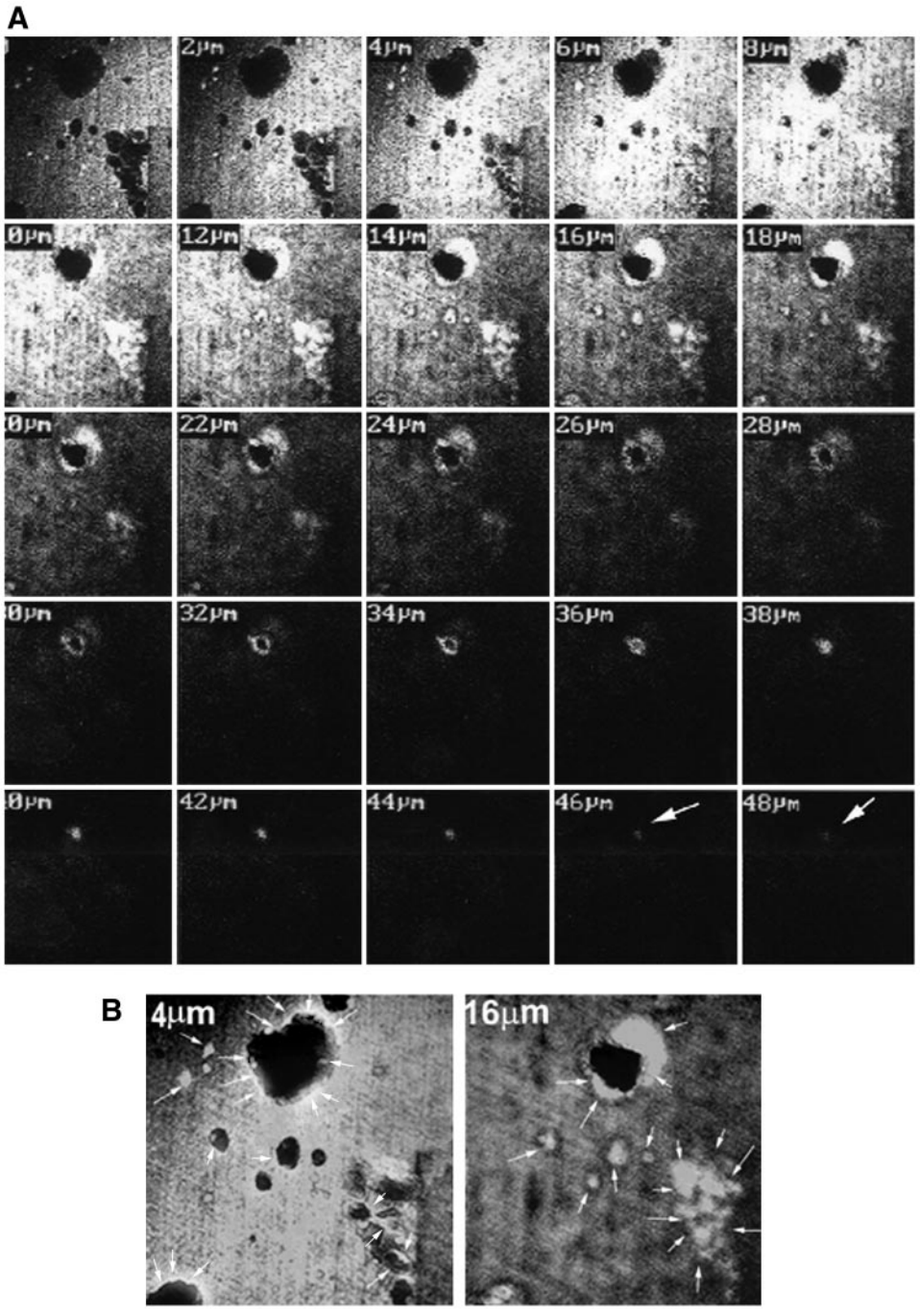

Figure 2. Distribution of OPN in dentine slices from which osteoclasts have been denuded. (A) A series of 2-μm YZ scans of the deepest resorption pit is shown. OPN staining is seen up to 48-μm section. Arrows (white) point to OPN localization. (B) Higher magnification of the sections demonstrates OPN staining at the rim (4 μm) and at the shoulder areas of the resorption pit (16 μm). Arrows (white) point to OPN localization at the rim in 4 μm, within the pit in 16-μm sections and at the bottom of the other pits. The results represent one of three experiments performed.

preparations, all demonstrating significant reductions in pit depth using osteoclasts from OPN−/− mice (Table 1). OPN addition to OPN−/− osteoclasts on dentine slices did not restore OPN to the surface of the pits, demonstrating that the added protein did not have access to the resorption space. Therefore, the OPN staining observed on the resorption surfaces (Figure 2) was most likely due to secretion from the ruffled border (Figure 1). These experiments demonstrate that deposition of OPN into the resorption pits enhances bone resorption and that its deficiency decreases bone resorption.

Motility Studies

To analyze whether OPN serves as critical ligand for osteoclast motility, we performed phagokinesis and transwell migration assays. Nondirectional osteoclast motility in response to OPN was analyzed by phagokinesis assays as

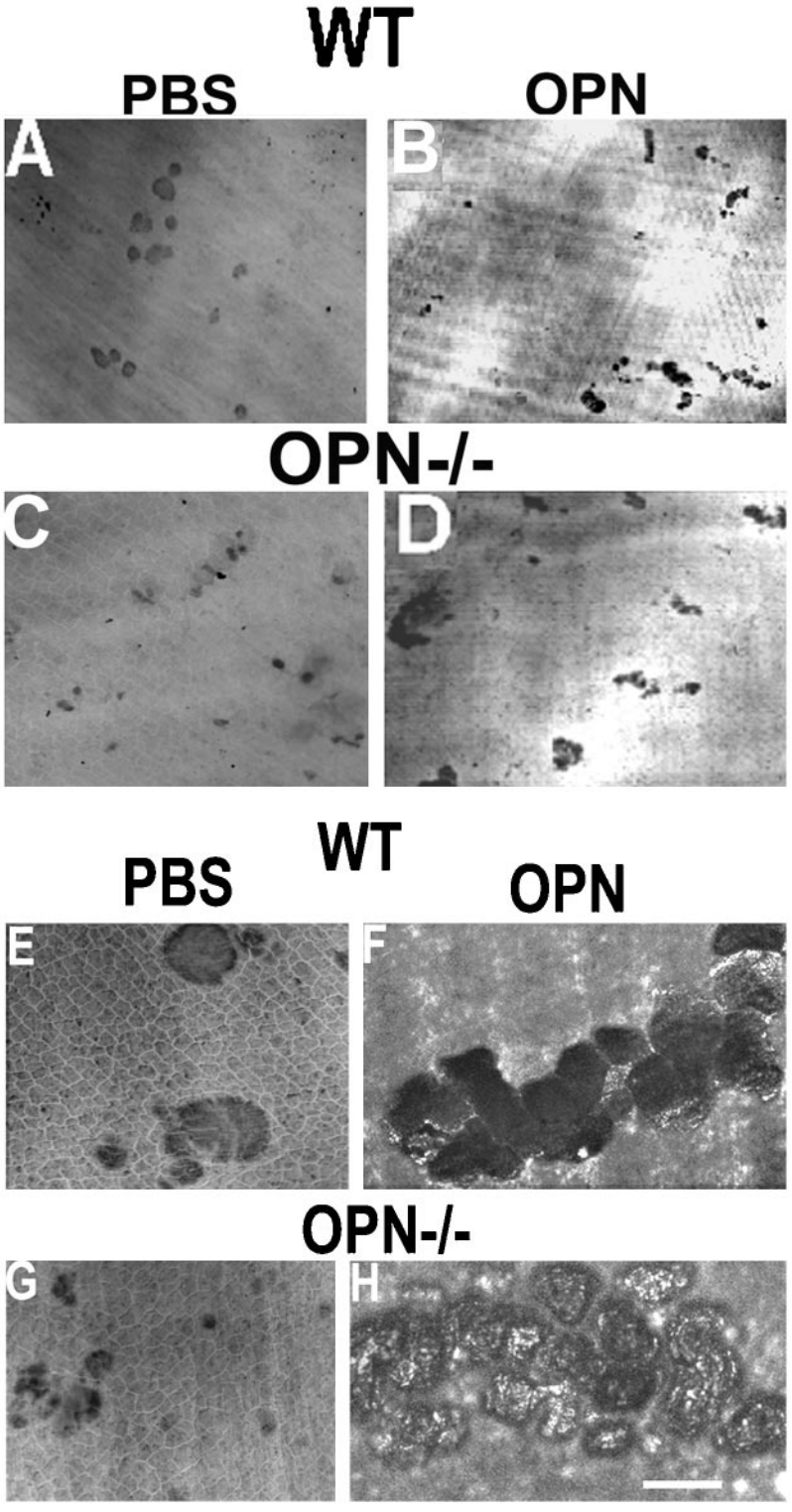

Figure 3. The effect of OPN on the bone resorption of WT and OPN−/− osteoclasts. Confocal microscopy analysis of the resorption pits on dentine slices. (A, B, E, and F) Wild-type osteoclasts; (C, D, G, and H) OPN-deficient osteoclasts. (A, C, E, and G) Osteoclasts treated with PBS (control); (B, D, F, and H) osteoclasts treated with OPN. (A–D) Lower power view of resorption pits using 10× objective. (E–H) Higher power magnification of resorption pits using 60× objective. Bar, 25 μm.

described in MATERIALS AND METHODS. Unstimulated osteoclasts derived from OPN−/− mice were significantly less motile than WT (Figure 4A). OPN stimulated migration significantly in osteoclasts isolated from both WT (solid bars) and OPN−/− (open bars) mice. The increase in migration stimulated by OPN in WT osteoclasts was 2.5-fold,

Table 1. Quantitation of resorption pits generated in vitro by osteoclasts from WT and OPN−/− mice

	WT		OPN−/−	
	PBS	OPN	PBS	OPN
Pit area (μm^2)	875 ± 128	3782 ± 563[a]	228 ± 78	3228 ± 317[b(a)]
Pit depth (μm)	11.5 ± 2.1[c]	38.7 ± 3.6[d]	3.5 ± 0.35	3.97 ± 0.74

About 10–15 pits/slice and three slices from each experiment were quantitated. Data are means ± SE of three experiments.

[a] $p < 0.001$; OPN of WT and OPN−/− osteoclasts versus PBS of WT osteoclasts.

[b] $p < 0.0001$-OPN versus PBS of OPN−/− osteoclasts.

[c] $p < 0.05$; PBS of WT versus PBS and OPN of OPN−/− osteoclasts.

[d] $p < 0.001$; OPN versus PBS of WT osteoclasts.

and in OPN−/− osteoclasts, it was 15–20-fold compared with the respective vehicle (PBS)-treated control osteoclasts. A 3–5-fold increase in osteoclast motility was observed in VN- or GRGDS-treated OPN−/− osteoclasts, whereas GRGDS or VN did not significantly increase the motility in WT osteoclasts. Anti-OPN antibodies significantly decreased phagokinetic movement in both WT and OPN−/− osteoclasts, which was not rescued by VN in WT cells. The reduction in motility below the basal level observed with PBS in the presence of neutralizing antibody to OPN indicates that basal rates of osteoclast motility are related to OPN secretion. The addition of anti-CD44 antibody also significantly inhibited OPN-stimulated phagokinesis.

Directional movement of osteoclasts toward chemoattractants was analyzed using transwell chambers. Filters of transwell chambers were coated with type I collagen, and chemotactic substrates were added to the lower chamber as indicated in Figure 4B. The migration rate with PBS in the lower chamber of OPN−/− osteoclasts was significantly lower than that of WT osteoclasts. Even though osteoclasts from OPN−/− mice responded to chemotactic factors in the lower chamber, the rate of migration related to WT osteoclasts was much lower. Thus, the OPN-deficient osteoclasts were clearly hypomotile. Neutralizing antibodies to $\alpha_v\beta_3$ and CD44 receptors produced results similar to anti-OPN antibodies.

Effects of OPN Deficiency on CD44 Expression

Because an interaction between CD44 and OPN has been suggested during chemotaxis (Weber *et al.*, 1996), we analyzed whether OPN deficiency affected CD44 expression. Immunostaining and confocal microscopy analysis of the distribution of CD44 protein in WT and OPN−/− osteoclasts are shown in Figure 5. The osteoclasts were immunostained before (Figure 5, B and D) and after (Figure 5, A and C) permeabilization with Triton X-100. Significant differences in the distribution of CD44 between WT and OPN−/− osteoclasts were discovered. A punctate dense basolateral membrane cell surface expression was observed in osteoclasts derived from WT mice (Figure 5B), which was markedly diminished in osteoclasts from OPN−/− mice (Figure 5D). In Triton-permeablized cells, there were no changes in the intensity of CD44 expression in osteoclasts derived from WT (Figure 5A) or OPN−/− (Figure 5C) mice. Dense CD44 staining was seen at the perinuclear region as

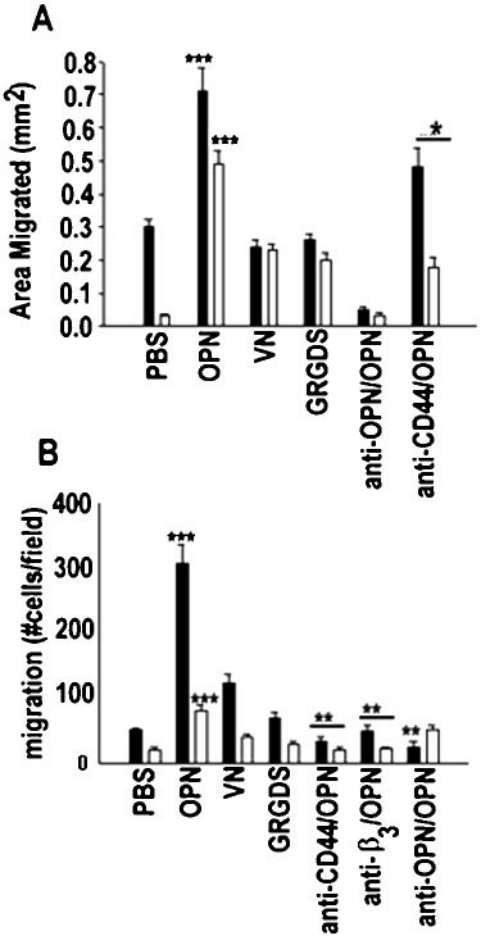

Figure 4. The effect of OPN on the motility of WT (■) and OPN−/− (□) osteoclasts. Motility of osteoclasts was assessed in vitro during both phagokinesis (A) and chemotaxis (B) assays. The treatments (OPN, 25 μg/ml; VN, 10 μg/ml; GRGDS, 50 μg/ml) are indicated at the bottom of the figures. Some cells were treated with an antibody to OPN, CD44, or integrin β3 (50 μg/ml) and OPN protein (25 μg/ml). The data are means ± SE (n = 3). ***$p < 0.0001$ vs. PBS; **$p < 0.001$ vs. OPN; *$p < 0.01$ vs. OPN.

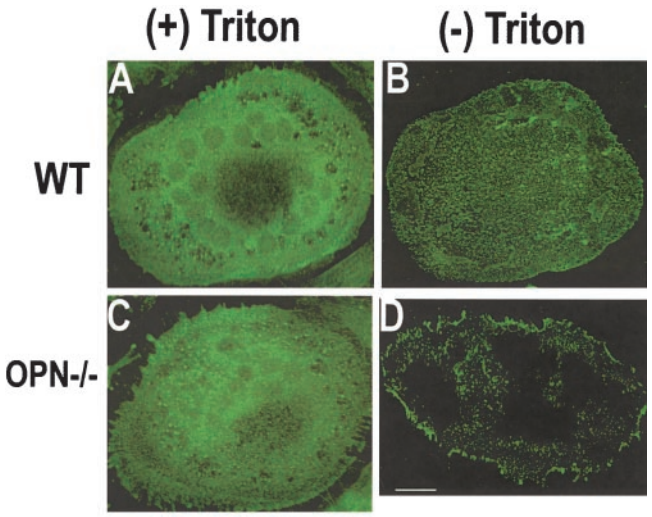

Figure 5. Immunolocalization of CD44 in osteoclasts isolated from WT (A and B) or OPN−/− (C and D) mice. Immunostaining with an antibody to CD44 was performed in Triton-permeablized (A and C) or nonpermeablized (B and D) osteoclasts. The results represent one of three experiments performed. Bar, 25 μm.

well as at the periphery of the cell closer to the plasma membrane in both WT (Figure 5A) and OPN−/− (Figure 5C) osteoclasts. These data correlated well with the results shown in Western analyses (Figure 6). Immunostaining for α_v or β_3 integrins demonstrated similar levels in osteoclasts from both WT and OPN−/− mice (unpublished data).

Effects of OPN Deficiency on $\alpha_v\beta_3$ and CD44 Expression

Because OPN deficiency decreased surface expression of CD44, we analyzed the expression levels of integrin $\alpha_v\beta_3$ and CD44 in WT and OPN−/− osteoclasts. Osteoclasts isolated from OPN−/− (Figure 6A, lanes 1, 3, 5, and 7) and WT (lanes 2, 4, 6, and 8) mice were surface-labeled with biotin and immunoprecipitated with either anti-β_3 (lanes 1and 2) or CD44 antibodies (lanes 5 and 6). Immunoprecipitates were blotted with streptavidin-HRP to visualize the surface expression of the receptors. Osteoclasts from OPN−/− mice had significantly decreased levels of CD44 surface expression (Figure 6A, lane 5), whereas the surface expression of integrin β_3 was the same in both OPN−/− (lane 1) and WT (lane 2) osteoclasts. To measure the cellular levels of CD44, the CD44 immunoblot (lanes 5 and 6) was stripped and blotted with an antibody to CD44. There were no changes in the cellular levels of CD44 in OPN−/− (lane 7) or WT (lane 8) osteoclasts, and only a single band of 85-kDa CD44 protein was detected. The 85-kDa standard CD44 (sCD44) protein is the smallest CD44 molecule lacking the entire variable region (Naot *et al.*, 1997), and sCD44 has a ubiquitous expression pattern.

Effects of OPN on CD44 Expression

The ability of OPN to stimulate CD44 surface expression was also examined in osteoclasts isolated from WT and OPN−/− mice. Osteoclasts were treated with PBS or OPN and surface labeled with biotin. The lysates were subjected to immunoprecipitation using an antibody to CD44. Immunoprecipitates were blotted with streptavidin-HRP to visualize the surface expression of receptors (Figure 6B, top panel). Osteoclasts from OPN−/− mice showed significantly decreased basal levels of CD44 surface expression and OPN stimulated surface expression of CD44 in both WT (lane 2) and OPN−/− (lane 4) osteoclasts. The blot shown in the top panel was stripped and immunoblotted with an antibody to CD44 to demonstrate the cellular levels of CD44 immunoprecipitated (Figure 6B, bottom panel). Only minor changes were observed in the cellular level of CD44 in PBS (bottom panel; lanes 1and 3) or OPN-treated (lanes 2 and 4) osteoclasts isolated from OPN−/− (lanes 3 and 4) or WT mice (lanes 1 and 2). In fact, more cellular CD44 protein was immunoprecipitated in both PBS- and OPN-treated osteoclasts isolated from OPN−/− mice.

These data are consistent with the significantly decreased levels of CD44 surface expression in osteoclasts from OPN−/− mice demonstrated in Figure 6A (lane 5), Figure 5D, and in studies designed to detect the presence of variant forms of CD44 (Figure 6C). To further confirm the expression of standard CD44 in osteoclasts, lysates were made from osteoclasts (Figure 6C, lanes 2, 3, 5, and 6) and melanoma cells (M21), a positive control for CD44 variants (lanes 1 and 4). Immunoprecipitates were prepared using antibodies to CD44s (lanes 1–3) or CD44 v3–10 (lanes 4–6). The higher molecular weight variant forms of CD44 were detected by a CD44 v3–10 antibody (BioSource International Inc.). We were unable to detect variant CD44 forms in osteoclasts (lanes 2, 3, 5, and 6) despite their detection in the positive control melanoma cells (M21; Figure 6C, lanes 1 and 4). The protein bands recognized by this antibody range from 85 to 250 kDa in melanoma cells, depending on glycosylation and the splice variant form of CD44 (indicated by asterisks). Results exactly similar to the data in Figures 5 and 6 were observed in four separate osteoclast preparations.

Role of Rho on CD44 Expression

CD44 and Rho-A are physically associated in vivo, and CD44 bound Rho A displays GTPase activity, which can be inhibited by C3-mediated ADP-ribosylation (Bourguignon *et al.*, 1999). We recently reported that transduction of constitutively active Rho^{val14} mimicked stimulation of osteoclast podosome assembly, motility, and bone resorption by OPN (Chellaiah *et al.*, 2000a). Therefore, we first examined whether activation of Rho by OPN occurred. After osteoclasts were treated with various treatments as indicated in Figure 7, surface biotinylation experiments was performed as described in MATERIALS AND METHODS. Results from a typical immunoblot of CD44 immunoprecpitates are shown in A and B. Figure 7A demonstrates the levels of surface expression of CD44 after various treatments. Treatment of osteoclasts with OPN stimulated CD44 surface expression both in OPN−/− (Figure 7A, lane 2) and WT (Figure 7A, lane 6) osteoclasts. Osteoclasts transduced with constitutively active Rho^{Val14} mimic the effects of OPN in both OPN−/− (lanes 3) and WT (lanes 7) osteoclasts, whereas the dominant negative Rho^{Asn19} (lane 9) did not have any effect on the increase in the CD44 surface expression. The Rho inhibitor, C3 exoenzyme blocked the effect of

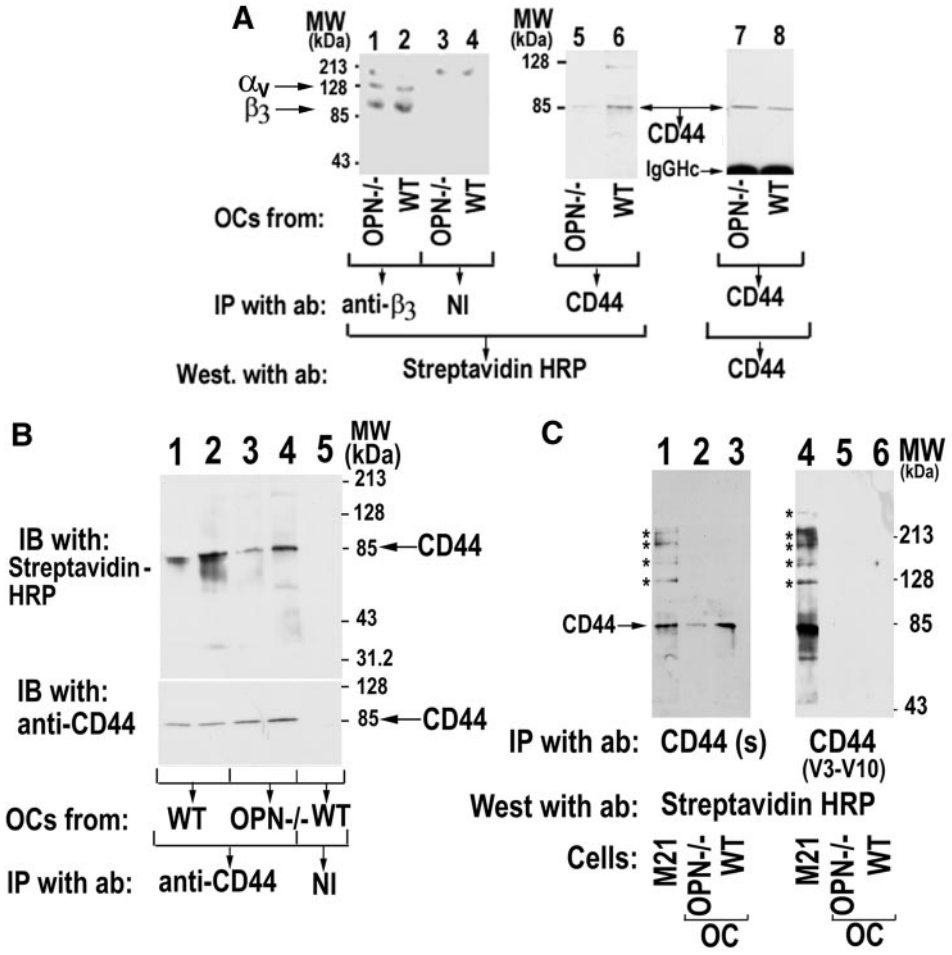

Figure 6. (A) Analysis of $\alpha_v\beta_3$ and CD44 expression in WT and OPN−/− osteoclasts. Osteoclasts isolated from OPN−/− (lanes 1, 3, 5, and 7) and WT (lanes 2, 4, 6, and 8) were surface-labeled with biotin and immunoprecipitated with either anti-β_3 (lanes 1 and 2) or anti-CD44 (lanes 5–8) antibodies. Immunoprecipitations with nonimmune serum (NI) are shown in lanes 3 and 4. Immunoprecipitates (lanes 1–6) were blotted with streptavidin-HRP to visualize the surface expression of the β_3 subunit (lanes 1 and 2) and CD44 (lanes 5 and 6). The CD44 immunoblot (lanes 5 and 6) was stripped and immunoblotted with anti-CD44 (antibody to the sCD44; BioSource International Inc.) and anti–rat, HRP-conjugated primary and secondary antibodies, respectively. Only a single band of 85-kDa CD44 protein was detected in equal amounts in both OPN-deficient (lane 7) and WT (lane 8) osteoclast lysates. Arrows point to the CD44, α_v, and β_3 proteins. The results shown are representative of three different experiments. (B) The effect of OPN on CD44 surface expression. Cell lysates made from PBS (lanes 1 and 3) or OPN–treated (lanes 2 and 4) osteoclasts isolated from WT (lanes 1, 2, and 5) or OPN−/− (lanes 3 and 4) mice were immunoprecipitated with anti-CD44 (lanes 1–4) or nonimmune serum (NI; lane 5). Immunoprecipitates were blotted with streptavidin-HRP to visualize the surface expression of CD44 (lanes 1–5, top panel). The immunoblot shown in the top panel was stripped and blotted with an sCD44 antibody (BioSource International Inc.) to demonstrate the cellular levels of CD44 immunoprecipitated (bottom panel). The results shown are representative of three independent experiments. (C) Analysis of CD44 variant expression in osteoclasts. Lysates were made from osteoclasts (lanes 2, 3, 5, and 6) and melanoma cells, a positive control for CD44 variants (lanes 1 and 4). Immunoprecipitates were prepared using antibodies to CD44s (lanes 1–3; antibody to the sCD44; BioSource International Inc.) or CD44 v3–10 (lanes 4–6; goat polyclonal anti-human CD44 variant, v3–10; BioSource International Inc). Immunoprecipitates were blotted with streptavidin-HRP to visualize the surface expression of CD44. The arrow indicates the band corresponding to the size of sCD44. Asterisks indicate the splice variant form of CD44. The results shown are representative of three independent osteoclast preparations and experiments.

Rho^{Val14} and decreased the CD44 surface expression level below basal level in both OPN−/− (Figure 7A, lane 4, and 7C) and WT (Figure 7A, lane 8, and 7C) osteoclasts. Figure 7C shows the densitometric scans of three independent experiments were expressed as percentage of CD44 surface expression. The surface expression level shown in each lane of Figure 7A was normalized to the corresponding total cellular levels of CD44 in Figure 7B. The percentage was calculated by comparing the various treatments of OPN−/− and WT osteoclasts to control, which refers to PBS-treated wild-type osteoclasts (Figure 7C). Rho^{Val-14} transduction stimulated CD44 surface expression significantly in OPN−/− osteoclasts but the effect was still lower than the effect observed in OPN-treated or Rho^{Val-14}-transduced (lane 6) osteoclasts isolated from wild-type mice. These data demonstrate a role for Rho in CD44 surface expression.

Role of Rho on Osteoclast Bone Resorption

Because Rho^{Val-14} transduction increases CD44 surface expression in OPN−/− osteoclasts, we analyzed the effects of Rho proteins on the bone resorption activity of osteoclasts from WT and OPN-deficient mice (Figure 8). Rho^{Val-14} transduction (C) had effects similar to OPN (B), and C3 exoenzyme (E) blocked the Rho effects in osteoclasts from both WT (Figure 8C) and OPN−/− (Figure 8I) mice.

The Effects of the Neutralizing Antibodies to OPN, β_3, and CD44 on OPN-induced Bone Resorption In Vitro

Osteoclasts derived from WT (Figure 9, top panel) and OPN−/− (bottom panel) mice were plated on dentine slices and treated as shown in Figure 9. Consistent with our pre-

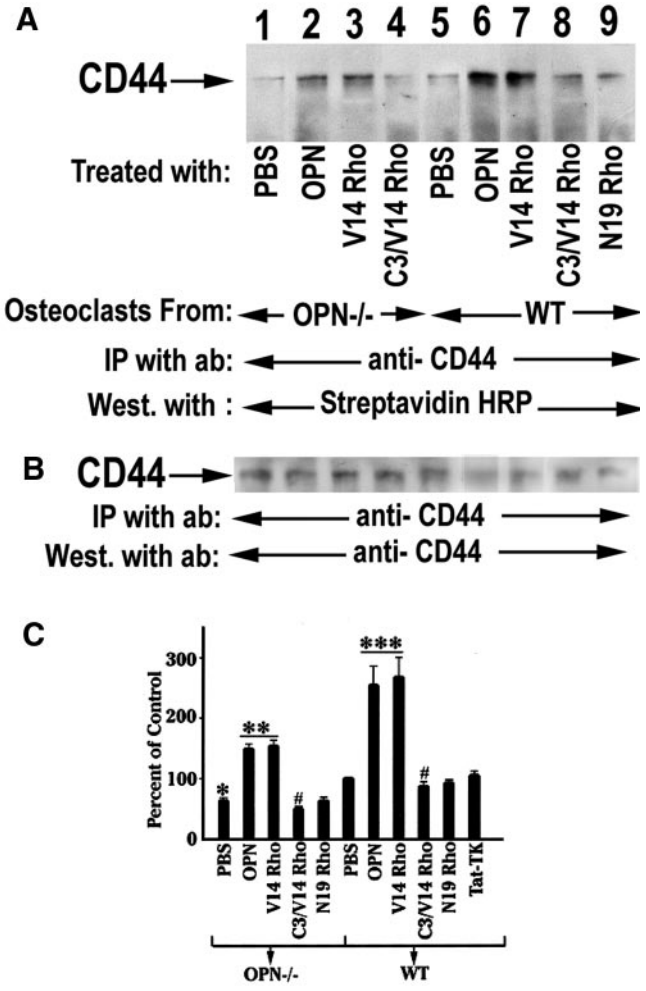

Figure 7. The effects of OPN or TAT-Rho protein transductions on CD44 surface expression. (A) Osteoclasts isolated from OPN−/− (lanes 1–4) and WT (lanes 5–9) mice were surface labeled with biotin after various treatments as indicated in the figure. The lysates were immunoprecipitated with an antibody to CD44. (A) Immunoprecipitates were blotted with streptavidin-HRP to visualize the surface expression of CD44. (B) The CD44 immunoblot was stripped and immunoblotted with anti-CD44 and anti-rat, HRP-conjugated primary and secondary antibodies, respectively. OPN (lanes 2 and 6) and Rho^{Val14} transduction increases surface expression of CD44 in both WT and OPN−/− osteoclasts. C3 exoenzyme blocked Rho^{Val14}-induced CD44 surface expression (lanes 4 and 8). (C) Densitometric scans of three experiments expressed as percent control are shown as mean ±. SEM ***$p < 0.0001$: OPN, V14 Rho vs. PBS of WT osteoclasts; **$p < 0.001$: OPN, V14Rho vs. PBS of OPN-deficient osteoclast; #$p < 0.01$: C3/V14 Rho vs. V14 rho of WT and OPN deficient osteoclast; *$p < 0.05$: PBS of OPN-deficient osteoclasts vs. PBS of WT osteoclasts.

vious (Chellaiah *et al.*, 2000b) and above observations (Figures 3 and 8), OPN stimulated the formation of multiple overlapping pits in both WT and OPN−/− osteoclasts (Figure 9, B and H). The increase in the area of pits in OPN-treated osteoclasts is due to increase in the simultaneous process of motility. The decrease in the OPN effect on the multiple overlapping pits formation by neutralizing antibodies to OPN (Figure 9, C and I), β_3 (Figure 9, D and J), or CD44 (Figure 9, F and L) in both WT and OPN−/− osteoclasts demonstrate that OPN-induced bone resorption is dependent on both $\alpha_v\beta_3$ and CD44 receptors. The above observations identify the critical role of Rho (Figure 8) as well as $\alpha_v\beta_3$ and CD44 receptors (Figure 9) in osteoclast function, under the influence of OPN-mediated signaling.

Skeletal Phenotype of the OPN−/− Mice

The results shown above demonstrate that OPN deficiency impairs osteoclast CD44 surface expression, motility, and bone resorption. The question then became whether these prominent effects on osteoclast function in vitro were related to a skeletal phenotype in vivo because they predicted a significant deficiency in osteoclast function.

In our laboratory facility, mutant OPN−/− mice were healthy for at least 18 months and showed normal somatic development and reproductive capacity, in agreement with the initial reports of the development of the null mice. OPN−/− mice behaved as expected and appeared to hear normally upon startling. Skeletal radiographs revealed no deformity of the long bones and are not shown. Femoral lengths were not altered, and the club-like deformities reported in the mild TRAP osteopetrotic mutations (Hayman *et al.*, 1996; Marks, 1989) were absent.

Assessment of Bone Morphology by pQCT

We analyzed the metaphyses of femurs using pQCT. These data for 12-week-old mice are summarized in Table 2. Trabecular bone area was significantly increased in the OPN−/− femurs compared with femurs from the wild-type animals ($p < 0.01$). The trabecular mineral density tended to be higher in OPN−/− mice but was not statistically significant. The cortical bone area in the metaphysis of OPN−/− mice was greater than that of WT mice ($p < 0.01$), but WT mice had significantly higher metaphyseal cortical bone mineral density than OPN−/− mice ($p < 0.05$). Thus, OPN deficiency was associated with an increase in femoral metaphyseal bone area.

Assessment of Bone Histomorphometry

For assessment of skeletal histomorphometry, mice were injected with calcein to label areas of bone mineralization on two occasions and histomorphometry of nondecalcified and decalcified bone sections was performed as described in MATERIALS AND METHODS. Tibial metaphyseal sections were stained or TRAP to aid in detection of osteoclasts. The trabeculae of OPN−/− bones were increased in number and thickness producing an increase in cancellous bone area (Table 3) in agreement with the pQCT measurements. Osteoclast number in the metaphyses was higher in bones from OPN−/− mice (Table 3). This increase may have been adaptive for the decreased bone resorption consistent with previous reports (Rittling *et al.* 1998; Yoshitake *et al.* 1999). The intensity of the TRAP stain did not differ between wild-type and mutant osteoclasts. The decrease in bone resorption of mutant mice was demonstrated by changes in eroded perimeters. The perimeters of eroded surfaces were significantly reduced in OPN−/− mice ($p < 0.05$), despite the

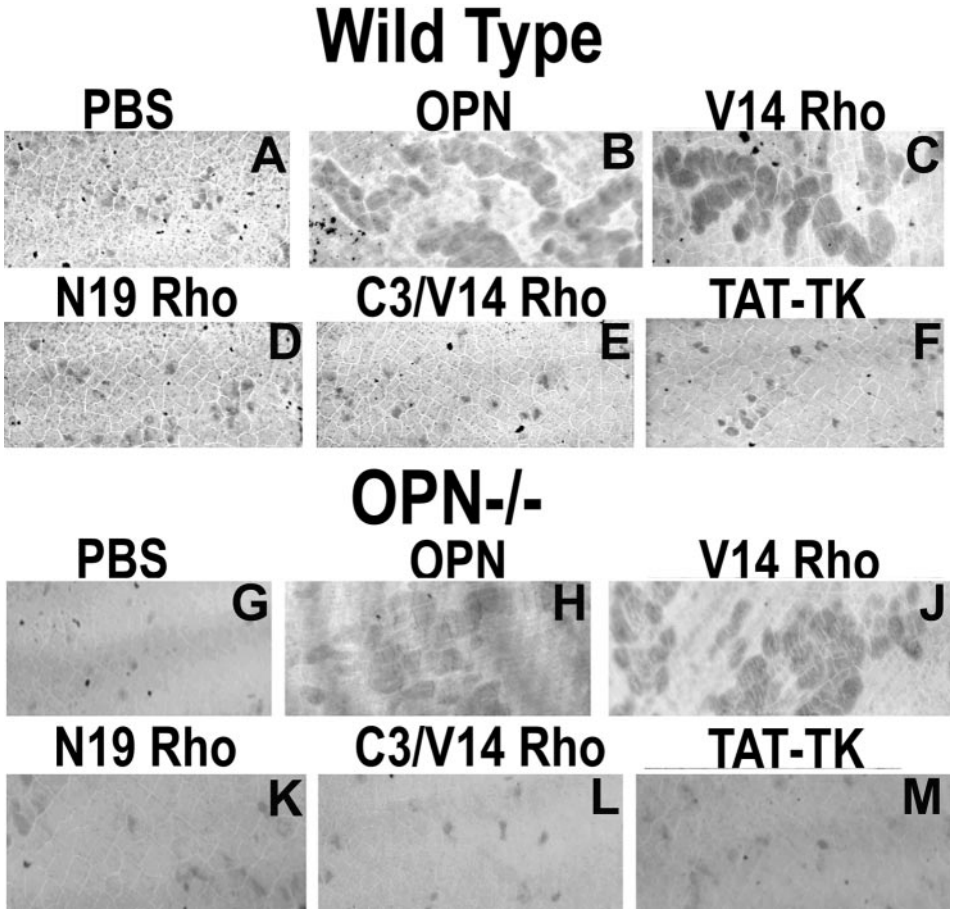

Figure 8. The effects of OPN or TAT-Rho protein transductions on bone resorption activity of WT and OPN-deficient osteoclasts. Osteocalsts isolated from WT and OPN−/− mice were treated as mentioned above each figure. Pits were viewed under 40× objective in a phase contrast microscope and photographed. OPN (B and H) and constitutively active $Rho^{Val\text{-}14}$ (C and J)-stimulated bone resorption activity compared with PBS- (A and G) or TAT-TK–transduced (F and M) control cells. Dominant negative $Rho^{Asn\text{-}14}$ (D and K) had no effect. C3 transferase (E and L) blocked $Rho^{Val\text{-}14}$-induced bone resorption activity significantly. The results represent one of the three experiments performed.

increase in osteoclast number, demonstrating that osteoclast-mediated bone resorption was diminished (Table 3). The osteoblastic parameters of bone modeling revealed no change in mineral apposition rate in OPN−/− mice, and bone formation rates were normal (Table 3). Thus, the increase in trabecular bone mass reported here probably resulted from the defect in bone resorption concomitant with a normal rate of bone formation, producing an imbalance in skeletal modeling and remodeling similar to that reported in mild osteopetrotic states (Hayman *et al.*, 1996; Chellaiah *et al.*, 2000b).

Mechanical Testing of OPN−/− Femurs

The histomorphometric findings of increased cancellous bone mass were analyzed further by load to failure testing in a four-point bending apparatus (Table 4). The OPN−/− femora were significantly stiffer (rigidity) and required a greater energy to produce failure. The cross-sectional moment of inertia was increased. The elastic modulus and ultimate periosteal tensile stress were increased in the OPN-deficient femurs.

DISCUSSION

The studies reported here demonstrate that OPN is expressed at the clear zone, basolateral and ruffled border plasma membrane surfaces of murine osteoclasts. Strongly positive immunostaining for OPN in newly excavated dentine surfaces demonstrated secretion into the bone resorption space. These data are consistent with those of Dodds *et al.* (1995), who demonstrated deposition of OPN into resorption pits on dentine slices, and Maeda *et al.* (1994), who also reported that OPN is preferentially present on the resorption lacunae formed by osteoclasts and that some osteoclasts trapped OPN on their surfaces.

Because osteoclasts express and secrete OPN, the question became what if any is the role of OPN in osteoclast function. We have previously reported that OPN stimulates bone resorption and osteoclast motility, increasing the number and depth of resorption pits produced by osteoclasts isolated from WT mice (Chellaiah *et al.*, 2000b). In this study we demonstrate that osteoclasts from OPN−/− mice are hypomotile and less active than WT osteoclasts in bone resorption. Thus, the function of secreted OPN, as an osteoclast autocrine factor, may be to stimulate cell motility and adhesion related to bone resorption. Osteoclasts are actively migrating cells, and hypomotility decreases bone resorption (Chellaiah *et al.*, 2000b). Adhesion, organization for migration, and organization for resorption are sequential events necessary for osteoclast function (Kanehisa and Heersche, 1988), and OPN stimulates each of these events. Also, addition of exogenous OPN to OPN−/− osteoclasts rescued

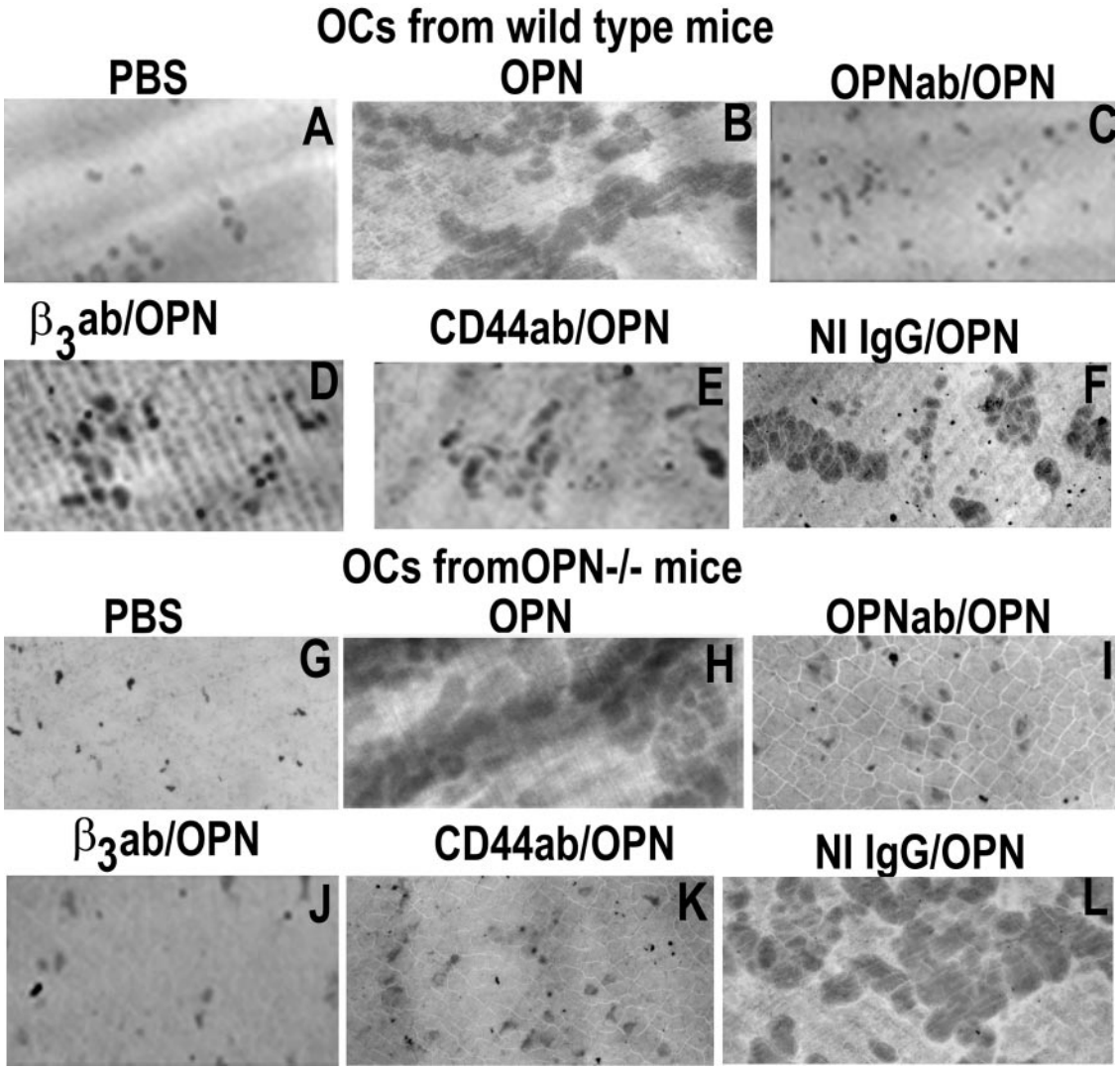

Figure 9. The effects of neutralizing antibodies to OPN, β_3, or CD44 on OPN- induced bone resorption. The effects of antibodies to OPN, β_3, or CD44 were assessed in OPN-induced bone resorption activity of osteoclasts isolated from WT (A–F) and OPN−/− (G–L) mice. OPN-induced bone resorption was reduced when cotreated with antibodies to β_3 (D and J), CD44 (E and K), or OPN (C and I) in both WT and OPN−/− osteoclasts. Osteoclasts treated with both nonimmune IgG and OPN (F and M) had similar effect as that of OPN-treatment (B and H). Pits were viewed under 40× objective in a phase contrast microscope and photographed. About three slices were used for each treatment. The experiment was repeated three times. The results represent one of the three experiments performed.

osteoclast phagokinesis and chemotaxis in vitro. A chemoattractant property of OPN has previously been demonstrated in macrophage and T-cell migration (O'Regan *et al.*, 1999).

OPN is a unique cytokine in that it stimulates both osteoclast motility and bone resorption. OPN deficiency results in small, superficial, and simple resorption pits on dentine slices produced by osteoclasts derived from OPN−/− mice. Stimulation by exogenous OPN increased the pit number and area formed by OPN−/− osteoclasts, but it was not sufficient to provide for normal resorption pit depth. That endogenous production of OPN is necessary for normal bone resorption is consistent with our previous studies (Chellaiah *et al.*, 2000b) and those of Tani-Ishii *et al.* (1997), who demonstrated that treatment of osteoclasts with anti-

Table 2. pQCT of femurs from 12-week-old WT and OPN−/− mice

Metaphyseal parameters	WT	OPN−/−
Trabecular area (mm^2)	0.72 ± 0.14	1.66 ± 0.33[a]
Trabecular density (mg/cm^3)	286 ± 64	379 ± 28
Cortical area (mm^2)	2.25 ± 0.19	2.34 ± 0.22[a]
Cortical density (mg/cm^3)	974 ± 47[b]	818 ± 39

The femoral bone density and area of WT and OPN−/− mice were calculated using a pQCT system as described in MATERIALS AND METHODS. [a] $p < 0.01$; [b] $p < 0.05$.

Table 3. Histomorphometry of bones from WT and OPN−/− mice

Tibial histomorphometry	WT	OPN−/−
Cancellous bone area (%)	16.2 ± 2.7	29.3 ± 5.3[a]
Trabecular spacing (μm)	195 ± 38.2	98.9 ± 7.6[b]
Trabecular number (No./mm)	4.79 ± 0.66	6.58 ± 0.44[b]
Trabecular thickness (μm)	28.1 ± 3.61	55.1 ± 4.68[c]
Number of osteoclasts (n)	76 ± 9.7	97 ± 2.2[b]
Osteoclasts/tissue area (No./mm^2)	134 ± 17	149 ± 12
Eroded perimeter (%)	4.56 ± 0.85	1.74 ± 0.69[a]
Mineral apposition rate (μm^2/μm/day)	1.50 ± 0.33	1.31 ± 0.14
Bone formation rate/bpm (μm^2/μm/day)	0.60 ± 0.17	0.54 ± 0.10

Longitudinal sections of the decalcified tibia were made. The sections were stained and the histomorphometric measurements were performed as described in MATERIALS AND METHODS. Data shown are means ± SE. There are 4 to 5 animals per group. [a] $p < 0.05$; [b] $p < 0.02$; [c] $p < 0.002$.

sense oligodeoxynucleotides to OPN results in inhibition of bone resorption by mouse osteoclasts in vitro. Moreover, other investigators have demonstrated inhibition of bone resorption by anti-OPN antibodies (Udagawa *et al.*, 1996).

The functions of OPN in osteoclasts include the promotion of cell adhesion during bone resorption (Reinholt *et al.*, 1990) and chemotaxis (Weber *et al.*, 1996; Weber, 2002). Dephosphorylation of OPN by TRAP may produce detachment of osteoclasts at the termination of resorption (Ek-Rylander *et al.*, 1994). Noda *et al.* (1998) have demonstrated that OPN-deficient bone matrix is poorly resorbed and has the diminished capacity to support cell adhesion to bone. OPN-deficient osteoclasts are less efficient in removing hydroxyapatite coated on glass and recruitment to ectopically implanted bone matrix. Osteopontin purified from bacteria, OPN phosphorylated in vitro using CKII enzyme, and eucaryotic OPN purified from human melanoma cells (M21 cells) transfected with OPN cDNA were added as soluble proteins to OPN−/− osteoclasts plated on dentine slices. These proteins had no effect in increasing the pit depth or rescuing the OPN deficiency in OPN−/− osteoclasts despite the fact that these osteoclasts demonstrated adhesion, polarization, and actin ring formation on dentine slices. To examine the effects of secretory OPN versus intracellular OPN, osteoclasts isolated from OPN−/− mice were either transfected with OPN cDNA or transduced with HA-TAT/OPN protein, respectively. OPN protein was detected in the culture medium of osteoclasts transfected with FL-OPN. An increase in pit depth and CD44 surface expression equal to wild-type osteoclasts was detected in OPN−/− osteoclasts transfected with OPN cDNA, whereas transduction of HA-TAT/OPN protein into osteoclasts had no effect in increasing the pit depth while partially rescuing CD44 surface expression. Transfection of OPN cDNA rescued OPN deficiency in CD44 surface expression and correcting pit depth (Chellaiah *et al.*, unpublished observations). These observations provide evidence to support OPN as a necessary osteoclast autocrine cytokine, regulating the sequential processes of migration, adhesion, and resorption that occur during bone resorption.

There is general agreement that OPN/$\alpha_v\beta_3$ interaction brings about the osteoclast adherence to the bone surface (Ross *et al.*, 1993), and the integrin, $\alpha_v\beta_3$ is localized in the sealing zone of osteoclasts and interacts with OPN in the bone matrix underneath (Flores *et al.*, 1992; Hughes *et al.*, 1993; Nesbitt *et al.*, 1993). Studies by Weber *et al.* (1996) have shown that OPN can mediate chemotaxis and attachment of monocytic cells through CD44 receptor. Therefore, we first studied the surface expression of CD44 and β_3 receptors in osteoclasts from WT and OPN−/− mice. CD44 surface expression is decreased in OPN-deficient osteoclasts, whereas the levels of the integrin receptor, $\alpha_v\beta_3$, were equal in both WT and OPN-deficient osteoclasts. Furthermore, OPN addition stimulated osteoclast chemotaxis through the $\alpha_v\beta_3$ integrin as shown here and previously (Chellaiah *et al.*, 2000a, 2000b). A neutralizing antibody to the integrin, β_3 blocked the rescue of CD44 surface expression by OPN demonstrating that signal transduction by $\alpha_v\beta_3$ is required for CD44 surface expression.

To further demonstrate that lack of autocrine stimulated signal transduction leading to decreased CD44 on the osteoclast surface was the basis of the OPN null phenotype, we analyzed whether activation of the key step in OPN-stimulated signal transduction would suffice to rescue the OPN-deficient osteoclast disability. We have shown that Rho activation is a critical step in the stimulation of motility by exogenous OPN (Chellaiah *et al.*, 2000a), and Rho is required in the intracellular trafficking of CD44 (Chellaiah, unpublished observations). We transduced constitutively active (Rho^{Val14}) and dominant negative Rho (Rho^{Asn19}) into oste-

Table 4. Mechanical strength of femurs from 12 week, WT and OPN−/− mice

Parameter	WT	OPN−/−
Rigidity (Nmm/[mm/mm^2])	909 ± 70	1308 ± 92[a]
Ultimate moment (Nmm)	28.8 ± 3.4	47.3 ± 2.0[a]
Ultimate normalized displacement (mm/mm^2)	0.042 ± 0.003	0.047 ± 0.003
Energy (Nmm* (mm/mm^2)	0.456 ± 0.12	1.1 ± 0.08[a]
Cross sectional moment of inertia (mm^4)	0.161 ± 0.010	0.191 ± 0.008[b]
Elastic modulus (GPa)	5.7 ± 0.19	7.1 ± 0.62[c]
Ultimate periosteal tensile stress (MPa)	116.1 ± 9.5 (n = 4)	170.7 ± 7.9[a] (n = 18)

Left femora from WT and OPN−/− mice were used for biomechanical testing. Four point bending tests were conducted using a materials testing machine as described in the MATERIALS AND METHODS. Data shown are means ± SE. [a] $p < 0.005$; [b] $p < 0.05$; [c] $p < 0.02$.

oclasts and demonstrated that Rho^{Val14} rescued CD44 surface expression, motility, and bone resorption activity in OPN−/− osteoclasts. The increase in the area of pits generated by Rho^{Val14} transduced OPN deficient osteoclasts is indicative of an increase in osteoclast motility function.

Our data regarding osteoclast CD44 are in agreement with Hughes *et al.* (1994) and Nakamura *et al.* (1995) who demonstrated CD44 in human and rat osteoclasts, respectively. Recent immunocytochemical studies have revealed colocalization of intracellular OPN with CD44 and ERM proteins in migrating embryonic fibroblastic cells, activated macrophages, and metastatic breast cancer cells. However, this association was based on OPN binding to an isoform of CD44 different from that expressed in osteoclasts (Sodek *et al.*, 2000; Zohar *et al.*, 2000). Thus, it is unclear whether OPN associates with CD44 during traffic to the membrane in osteoclasts, but because exogenous OPN was able to rescue CD44 surface expression in OPN−/− osteoclasts, this does not appear to be a critical association.

The impairment in bone resorption produced in vitro by OPN deficiency indicated a probable defect in osteoclast function in OPN-null mutant mice in vivo. Indeed, we found by histomorphometry an increase in cancellous bone area, trabecular bone thickness, and a decrease in trabecular spacing compatible with impaired function of osteoclasts in OPN−/− mice. Eroded perimeters of trabeculae were diminished despite increased osteoclast number. It has been shown that OPN−/− mice have increased capacity to make osteoclasts from spleen cells (Rittling *et al.*, 1998). Our histomorphometric analyses demonstrated that the osteoclast number was greater in the bones of OPN−/− mice compared with WT mice. The increase in osteoclast number may be compensatory for the decreased activity of OPN−/− osteoclasts. The increase in number of osteoclasts may be due to an increase in RANKL expression in the bones of OPN−/− mice (Yoshitake *et al.*, 1999). The increase in bone mass was confirmed by pQCT measurements that showed an increase in trabecular bone area. This indicates that OPN deficiency, via defective osteoclast-mediated bone resorption, leads to increased bone mass. The mechanical properties of the OPN−/− femora demonstrated increased stiffness, requiring greater energy to fracture. Thus, targeting OPN stimulated bone resorption might strengthen the skeleton.

The defect in OPN-deficient osteoclast function was insufficient to affect endochondral bone growth, and the shortening and clubbing of the femurs reported in some osteopetrotic states was not observed (Marks, 1989; Hayman *et al.*, 1996). These data are consistent with reports demonstrating that OPN deficiency impaired activation of osteoclasts in estrogen deficiency, PTH stimulation, and RANKL stimulation (Yoshitake *et al.*, 1999; Ihara *et al.*, 2001). Although Rittling *et al.* (1998) did not report formal bone histomorphometry, an increase in trabecular bone volume was observed by Yoshitake *et al.* (1999), consistent with our studies. Thus, the findings reported herein of thickened calcified trabeculae, delayed resorption, and diminished eroded perimeters demonstrate a mild defect in osteoclast function that was neither developmentally important nor sufficient to affect growth, but it was sufficient to increase trabecular and cortical bone thickness with age. The findings reported here are similar to the osteopetrosis of gelsolin deficiency (Chellaiah *et al.*, 2000b), and they resemble the long-term outcome of aminobisphosphonate administration to humans, producing a mild imbalance between bone resorption and bone formation that results in an increase in bone mass (Liberman, 1995; Saag *et al.*, 1998). Osteopetrosis is a heterogenous group of disorders, which range in severity from lethal to the very mild disorder as reported here. The milder form of osteopetrosis has been associated with significant effects on skeletal mineralization, demonstrating progressive increases in bone density (Hayman *et al.*, 1996) as observed here by the increase in trabecular bone density.

Osteopetrotic phenotype was also identified in transgenic mice developed by disruption of c-Src (Soriano *et al.*, 1991) or c-Fos gene (Wang *et al.*, 1991). Osteopetrotic phenotype in these mice are due to either inactive or absence of osteoclasts, respectively. Similarly, the mutation responsible for the microopthalmic (mi) mouse osteopetrosis has been identified in the gene encoding a novel member of the basic-helix-loop-helix-helix leucine zipper (bHLH-ZIP) protein family of transcriptional factors. A defect in the fusion process of osteoclast precursor cells was detected in these mice (Chambers and Loutit, 1979; Minkin, 1981). Mice with no biologically active CSF-1 developed osteopetrotic phenotype due to almost complete lack of osteoclast and impaired bone resorption (Naito *et al.*, 1991; Cecchini *et al.*, 1994). In humans, deficiency of carbonic anhydrase II is identified as the primary defect in the autosomal recessive syndrome of osteopetrosis with renal tubular acidosis and cerebral calcification (Sly *et al.*, 1983; reviewed in Felix *et al.*, 1996). These observations demonstrate the genetic effects of some osteopetrotic mutations and their relevance to the development and function of osteoclasts. The OPN null mice demonstrate a milder osteopetritic phenotype due to deficiency in CD44 surface expression resulting in defective motility and bone resorptive functions of osteoclasts.

Our data show that OPN is a required osteoclast motility factor mediating surface expression of CD44 receptor. Also, OPN secreted into the resorption pit is required for adhesion during bone resorption. Osteoclast-like cells derived from peripheral blood of osteopetrotic patients and normal individuals demonstrated similar morphology but alterations in the expression of CD44. These osteoclasts were defective in bone resorption function (Flanagan *et al.*, 2000). Spatial and temporal patterns of OPN/CD44 expression were seen in the healing fractures of rat femora. In the remodeling callus, CD44 expression was detected on the basolateral plasma membrane of osteoclasts, osteocyte lacunae but not in the cuboidal osteoblasts. It was shown that OPN is the major ligand for CD44 on bone cells in the remodeling phase of healing fractures and CD44/OPN interaction has clinical implications in the repair of skeletal tissues (Yamazaki *et al.*, 1999). The decrease in CD44 expression in osteopetrotic patients (Flanagan *et al.*, 2000) and in OPN−/− mice that are mildly osteopetrotic implicates the role of CD44 in osteoclast function and bone modeling. Our data demonstrate the required roles of OPN in osteoclast function and provide new insights into the role of $\alpha_v\beta_3$ and CD44 receptors in osteoclast function and disordered bone modeling. We have also demonstrated that OPN/$\alpha_v\beta_3$ generated outside-in Rho signaling pathway is required for the surface expression of CD44 as well as CD44 associated signaling complex formation. Osteoclast motility requires both $\alpha_v\beta_3$ and CD44 recep-

tors. Surface expression of CD44 can influence multiple pathways that are crucial for osteoclast motility.

ACKNOWLEDGMENTS

This work was supported by National Institutes of Health (NIH) grants AR46292 (M.A.C.), AR41677 (K.A.H.), DK09976 (K.A.H.), AR39561 (K.A.H.), AR44434 (D.T.D.), ES06897 (D.T.D.), and CA72740 (S.R.R.); by a grant from the Washington University/Pharmacia consortium; and by a grant from the University of Maryland, Dental School (DRIF). The NIH grants (AR44434 and ES06897) generously supported work on the OPN-deficient mice at Rutgers University.

REFERENCES

Bourguignon, L.Y., Zhu, H., Shao, L., Zhu, D., and Chen, Y.W. (1999). Rho-kinase (ROK) promotes CD44v (3, 8–10) ankyrin interaction and tumor cell migration in metastatic breast cancer cells. Cell Motil. Cytoskel. *43*, 269–287.

Cecchini, M.G., Dominigues, M.G., Mocci, S., Wetterwald, A., Felix, R., and Fleich, H. (1994). Role of colony-stimulating factor-1 in the establishment and regulation of tissue macrophages during postnatal development of the mouse. Development *120*, 1367–1372.

Chambers, T.J., and Loutit, J.F. (1979). A functional assessment of macrophages from osteopetrotic mice. J. Pathol. *129*, 57–63.

Chellaiah, M., and Hruska, K. (2002). The integrin $\alpha_v\beta_3$, and CD44 regulate the actions of osteopontin on osteoclast motility. Calcif. Tissue Int. (*in press*).

Chellaiah, M., Biswas, R.S., Yuen, D., Alvarez, U.M., and Hruska, K. (2001). Phosphoinositol 3,4,5-trisphosphate directs association of SH2 containing signaling proteins with gelsolin. J. Biol. Chem. *276*, 47434–47444.

Chellaiah, M., Fitzgerald, C., Filardo, E.J., Cheresh, D.A., and Hruska, K.A. (1996). Osteopontin activation of c-*src* in human melanoma cells requires the cytoplasmic domain of the integrin α_v subunit. Endocrinology *137*, 2432–2440.

Chellaiah, M., and Hruska, K.A. (1996). Osteopontin stimulates gelsolin associated phosphoinositide levels and PtdIns 3-hydroxyl kinase. Mol. Biol. Cell *7*, 743–753.

Chellaiah, M., Kizer, N., Silva, M., Alvarez, U., Kwiatkowski, D., and Hruska, K.A. (2000b). Gelsolin deficiency blocks podosome assembly and produces increased bone mass and strength. J. Cell Biol. *148*, 665–678.

Chellaiah, M., Soga, N., Swanson, S., McAllister, S., Alvarez, U., Wang, D., Dowdy, S.F., and Hruska, K.A. (2000a). Rho-A is critical for osteoclast podosome organization, motility, and bone resorption. J. Biol. Chem. *275*, 11993–12002.

Chenu, C. *et al.* (1994). Osteocalsin induces chemotaxis, secretion of matrix proteins, and calcium-mediated intracellular signaling in human osteoclast-like cells. J. Cell Biol. *127*, 1149–1158.

Denhardt, D.T., Noda, M., O'Regan, W., Pavlin, D., and Berman, J.S. (2002). Osteopontin as a means to cope with environmental insults: regulation of inflammation, tissue remodeling, and cell survival. J. Clin. Invest. *107*, 1055–1061.

Dodds, R.A., Connor, J.R., James, I.E., Rykaczewski, E.L., Appelbaum, E., Dul, E., Gowen, M. (1995). Human osteoclasts, not osteoblasts, deposit osteopontin onto resorption surfaces: an in vitro and ex vivo study of remodeling bone. J. Bone Miner. Res. *10*, 1666–1680.

Ek-Rylander, B., Flores, M., Wendel, M., Heinegard, D., and Andersson, G. (1994). Dephosphorylation of osteopontin and bone sialoprotein by osteoclastic tartrate-resistant acid phosphatase. J. Biol. Chem. *269*, 14853–14856.

Felix, R., Hofstetter, W., and Cecchini, M.G. (1996). Recent developments in the understanding of the pathophysiology of osteopetrosis. Eur. J. Endocrinol. *134*, 143–156.

Flanagan, A.M., Sarma, U., Steward, C.G., Vellodi, A., and Horton, M.A. (2000). Study of the nonresorptive phenotype of osteoclast-like cells from patients with malignant osteopetrosis: a new approach to investigating pathogenesis. J. Bone Miner. Res. *15*, 352–360.

Flores, M.E., Norgard, M., Heinegard, D., Reinholt, F.P., and Andersson, G. (1992). RGD-directed attachment of isolated rat osteoclasts to osteopontin, bone sialoprotein, and fibronectin. Exp. Cell Res. *201*, 526–530.

Hayman, A.R., Jones, S.J., Boyde, A., Foster, D., Colledge, W.H., Carlton, M.B., Evans, M.J., and Cox, T.M. (1996). Mice lacking tartrate-resistant acid phosphatase (Acp 5) have disrupted endochondral ossification and mild osteopetrosis. Development *122*, 3151–3162.

Hughes, D.E., Salter, D.M., Dedhar, S., and Simpson, R. (1993). Integrin expression in human bone. J. Bone Miner. Res. *8*, 527–533.

Hughes, D.E., Salter, D.M., and Simpson, R. (1994). CD44 expression in human bone: a novel marker of osteocytic differentiation. J. Bone Miner. Res. *9*, 39–44.

Hultenby, K., Reinholt, F.P., Oldberg, A., and Heinegard, D. (1991). Ultrastructural immunolocalization of osteopontin in metaphyseal and cortical bone. Matrix *11*, 206–213.

Ihara, H. *et al.* (2001). Parathyroid hormone-induced bone resorption does not occur in the absence of osteopontin. J. Biol. Chem. *276*, 13065–13071.

Ikeda, T., Nomura, S., Yamaguchi, A., Suda, T., and Yoshiki, S. (1992). In situ hybridization of bone matrix proteins in undecalcified adult rat bone sections. J. Histochem. Cytochem. *40*, 1079–1088.

Jilka, R.L., Weinstein, R.S., Takahashi, K., Parfitt, A.M., and Manolagas, S.C. (1996). Linkage of decreased bone mass with impaired osteoblastogenesis in a murine model of accelerated senescence. J. Clin. Invest. *97*, 1732–1740.

Kanehisa, J., and Heersche, J.N.M. (1988). Osteoclastic bone resorption: In vitro analysis of the rate of resorption and migration of individual osteoclasts. Bone *9*, 73–79.

Lakkakorpi, P.T., and Vaananen, H.K. (1991). Kinetics of the osteoclast cytoskeleton during the resorption cycle *in vitro*. J. Bone Miner. Res. *6*, 817–826.

Liaw, L., Almeida, M., Hart, C.E., Schwartz, S.M., and Giachelli, C.M. (1994). Osteopontin promotes vascular cell adhesion and spreading and is chemotactic for smooth muscle cells *in vitro*. Circ. Res. *74*, 214–224.

Liberman, U.A. (1995). Effect of oral alendronate on bone mineral density and the incidence of fractures in postmenopausal osteoporosis. New Engl. J. Med. *333*, 1437–1443.

Maeda, M., Kukita, T., Akamine, A., Kukita, A., and Iijima, T. (1994). Localization of osteopontin in resorption lacunae formed by osteoclast-like cells: a study by a novel monoclonal antibody which recognizes rat osteopontin. Histochemistry *102*, 247–254.

Mark, M.P., Prince, C.W., Oosawa, T., Gay, S., Bronkers, A.L.J., and Butler, W.T. (1987). Immunohistochemical demonstration of a 44 kd phosphoprotein in developing rat bones. J. Histochem. Cytochem. *35*, 707–715.

Marks, S.C., Jr. (1989). Osteoclast biology: lessons from mammalian mutations. Am. J. Med. Genet. *34*, 43–54.

McKee, M.D., Farach, C.M., Butler, W.T., Hauschka, P.V., Nanci, A. (1993). Ultrastructural immunolocalization of noncollagenous (osteopontin and osteocalcin) and plasma (albumin and alpha 2HS-glycoprotein) proteins in rat bone. J. Bone Miner. Res. *8*, 485–496.

McKee, M.D., and Nanci, A. (1996). Osteopontin: an interfacial extracellular matrix protein in mineralized tissues. Connect. Tissue Res. *35*, 197–205.

Merry, K., Dodds, R., Littlewood, A., and Gowen, M. (1993). Expression of osteopontin mRNA by osteoclasts and osteoblasts in modeling adult human bone. J. Cell Sci. *104*, 1013–1020.

Minkin, C. (1981). Defective macrophage chemotaxis in osteopetrotic mice. Calcif. Tissue Int. *33*, 677–678.

Naito, M., Hayashi, S.I., Yoshida, H., Nishikawa, S.I., Schultz, I.D., and Takahashi, K. (1991). Abnormal differentiation of tissue macrophage populations in 'osteopetrosis' (OP) mice defective in the production of macrophage colony stimulating factor. Am. J. Pathol. *139*, 657–666.

Nakamura, H., Kenmotsu, S.-I., Sakai, H., and Ozawa, H. (1995). Localization of CD44, the hyaluronate receptor, on the plasma membrane of osteocytes and osteoclasts in rat tibiae. Cell Tissue Res. *280*, 225–233.

Nakamura, I., Gailit, J., and Sasaki, T. (1996). Osteoclast integrin alphaVbeta3 is present in the clear zone and contributes to cellular polarization. Cell Tissue Res. *286*, 507–515.

Naot, D., Sionov, R.V., and Ish-Shalo, D. (1997). CD44: structure, function, and association with the malignant process. Adv. Cancer Res. *71*, 241–319.

Nesbitt, S., Nesbit, A., Helfrich, M., and Horton, M. (1993). Biochemical characterization of human osteoclast integrins. Osteoclasts express alpha v beta 3, alpha 2 beta 1, and alpha v beta 1 integrins. J. Biol. Chem. *268*, 16737–16745.

Noda, M. *et al.* (1998). Osteopontin deficient mice (OD−) cells exhibit enhanced actin fiber formation and spreading while OD− osteoclasts are less efficient in removing hydroxyapatite coated on glass and in recruitment to ectopically implanted bone matrix. J. Bone Miner. Res. *23*, S220.

O'Regan, A.W., Chupp, G.L., Lowry, J.A., Goetschkes, M., Mulligan, N., and Berman, J.S. (1999). Osteopontin is associated with T cells in sarcoid granulomas and has T cell adhesive and cytokine-like properties in vitro. J. Immunol. *162*, 1024–1031.

Parfitt, A.M., Drezner, M.K., Glorieux, F.H., Kanis, J.A., Malluche, H., Meunier, P.J., Ott, S.M., and Recker, R.R. (1987). Bone histomorphometry: standardization of nomenclature, symbols, and units. J. Bone Miner. Res. *2*, 595–610.

Reinholt, F.P., Hultenby, K., Oldberg, A., and Heinegard, D. (1990). Osteopontin—a possible anchor of osteoclasts to bone. Proc. Natl. Acad. Sci. USA *87*, 4473–4475.

Rittling, S.R. *et al.* (1998). Mice lacking osteopontin show normal development and bone structure but display altered osteoclast formation in vitro. J. Bone Miner. Res. *13*, 1101–1111.

Ross, F.P. *et al.* (1993). Interaction between the bone matrix proteins osteopontin and bone sialoprotein and the osteoclast integrin $\alpha_v\beta_3$ potentiate bone resorption. J. Biol. Chem. *268*, 9901–9907.

Saag, K.G. *et al.* (1998). Alendronate for the prevention and treatment of glucocorticoid-induced osteoporosis. New Engl. J. Med. *339*, 292–299.

Senger, D.R., Ledbetter, S.R., Claffey, K.P., Papadopoulos-Sergiou, A., Perruzzi, C.A., Detmar, M. (1996). Stimulation of endothelial cell migration by vascular permeability factor/vascular endothelial growth factor through cooperative mechanisms involving the $\alpha_v\beta_3$ integrin, osteopontin, and thrombin. Am. J. Pathol. *149*, 293–305.

Sly, W.S., Hewette-Emmett, D., Whyte, M.P., Yu, Y.S.I., and Tushian, R.E. (1983). Carbonic anhydrase II deficiency identified as the primary defect in the autosomal recessive syndrome of osteopetrosis with renal tubular acidosis and cerebral calcification. Proc. Natl. Acad. Sci. USA *80*, 2753–2756.

Sodek, J., Ganss, B., and McKee, M.D. (2000). Osteopontin. Crit. Rev. Oral Biol. Med. *11*, 279–303.

Soga, N., Connolly, J., Chellaiah, M., Kawamura, J., and Hruska, K.A. (2001). Rac regulates vascular endothelial growth factor stimulated motility. Cell Adhes. Commun. *8*, 1–13.

Soriano, P., Montgomery, X., Geske, R., and Bradely, A. (1991). Targeted disruption of the c-Src proto-oncogene leads to osteopetrosis in mice. Cell *64*, 693–702.

Suzuki, K., Zhu, B., Rittling, S.R., Denhardt, D.T., Goldberg, H.A., McCulloch, C.A., and Sodek, J. (2002). Colocalization of intracellular osteopontin with CD44 is associated with migration, cell fusion, and resorption in osteoclasts. J. Bone Miner. Res. *17*, 1486–1497.

Takaishi, K., Sasaki, T., and Taka, L. (1995). Cell motility assay and inhibition by Rho-GDP dissociation inhibitor. Methods Enzymol. *256*, 336–347.

Takano-Yamamoto, T., Takemura, T., Kitamura, Y., Nomura, S. (1994). Site-specific expression of mRNAs for osteonectin, osteocalcin, and osteopontin revealed by in situ hybridization in rat periodontal ligament during physiological tooth movement. J. Histochem. Cytochem. *42*, 885–896.

Tani-Ishii, N., Tsunoda, A., and Umemoto, T. (1997). Osteopontin antisense deoxyoligonucleotides inhibit bone resorption by mouse osteoclasts *in vitro*. J. Periodont. Res. *32*, 480–486.

Tezuka, K. *et al.* (1992). Identification of osteopontin in isolated rabbit osteoclasts. Biochem. Biophys. Res. Commun. *186*, 911–917.

Udagawa, N., Findlay, D.M., and Martin, T.J. (1996). CD44 involvement in osteoclast differentiation as well as bone resorption by mature osteoclasts. J. Bone Miner. Res. *11*, S112.

Wang, Z.O., Grigoriadis, A.E., MohlSteinlein, U., Ruther, U., and Wagner, E.F. (1991). A novel target cell for c-fos induced oncogenesis: development of chondrogenic tumors in embryonic stem cell chimeras. EMBO J. *10*, 2437–2450.

Weber, G.F., Ashkar, S., Glimcher, M.J., and Cantor, H. (1996). Receptor-ligand interaction between CD44 and osteopontin (Eta-1). Science *271*, 509–512.

Weber, G.F. (2002). The metastasis gene osteopontin: a candidate target for cancer therapy. Biochem. Biophys. Acta *1552*, 61–85.

Weinreb, M., Shinar, D., and Rodan, G.A. (1990). Different pattern of alkaline phosphatase, osteopontin, and osteocalcin expression in developing rat bone visualized by in situ hybridization. J. Bone Miner. Res. *5*, 831–842.

Weinstein, R.S., Jilka, R.L., Parfitt, A.M., and Manolagas, S.C. (1997). The effects of androgen deficiency on murine bone remodeling and bone mineral density are mediated via cells of the osteoblastic lineage. Endocrinology *138*, 4013–4021.

Yamazaki, M., Nakajima, F., Ogasawara, A., Moriya, H., Majeska, R.J., and Einhorn, T.A. (1999). Spatial and temporal distribution of CD44 and osteopontin in fracture callus. J. Bone Joint Surg. Br. *81*, 508–515.

Yoshitake, H., Rittling, S.R., Denhardt, D.T., and Noda, M. (1999). Osteopontin-deficient mice are resistant to ovariectomy-induced bone resorption. Proc. Natl. Acad. Sci. USA *96*, 8156–8160.

Zhao, H., Laitala-Leinonen, T., Parikka, V., and Vaananen, H.K. (2001). Downregulation of small GTPase Rab7 impairs osteoclast polarization and bone resorption. J. Biol. Chem. *276*, 39295–39302.

Zohar, R., Suzuki, N., Suzuki, K., Arora, P., Glogauer, M., McCulloch, C.A., and Sodek, J. (2000). Intracellular osteopontin is an integral component of the CD44-ERM complex involved in cell migration. J. Cell Physiol. *184*, 118–130.